Two-group Poisson-Dirichlet mixtures for multiple testing

Francesco Denti
fdenti@uci.edu
Department of Statistics, University of California, Irvine

Michele Guindani
michele.guindani@uci.edu
Department of Statistics, University of California, Irvine

Fabrizio Leisen
F.Leisen@kent.ac.uk
School of Mathematics, Statistics and Actuarial Sciences,
University of Kent, Canterbury, UK

Antonio Lijoi
antonio.lijoi@unibocconi.it
Department of Decision Sciences, Bocconi University, Milan Italy
Bocconi Institute of Data Science and Analytics (BIDSA)

W. Duncan Wadsworth
duwads@microsoft.com
Microsoft, Redmond, Washington

Marina Vannucci
marina@rice.edu
Department of Statistics, Rice University, Houston, Texas

June 4, 2020

The simultaneous testing of multiple hypotheses is common to the analysis of high-dimensional data sets. The two-group model, first proposed in Efron [2004], identifies significant comparisons by allocating observations

to a mixture of an empirical null and an alternative distribution. In the Bayesian nonparametrics literature, many approaches have suggested using mixtures of Dirichlet Processes in the two-group model framework. Here, we investigate employing mixtures of two-parameter Poisson Dirichlet Processes (2PPD) instead, and show how they provide a more flexible and effective tool for large-scale hypothesis testing. Our model further employs non-local prior densities to allow separation between the two mixture components. We obtain a closed form expression for the exchangeable partition probability function of the two-group model, which leads to a straightforward MCMC implementation. We compare the performance of our method for large-scale inference in a simulation study and illustrate its use on both a prostate cancer dataset and a case-control microbiome study of the gastrointestinal tracts in children from underdeveloped countries who have been recently diagnosed with moderate to severe diarrhea.

Keywords: B ayesian nonparametrics, Microbiome analysis, Multiple testing, Poisson–Dirichlet process, Two-group model

1 Introduction

The availability of high-dimensional data in domains as diverse as genomics, imaging, and astronomy, has brought the necessity to screen a large number of hypotheses simultaneously. Here, we focus on the two-group modeling framework [Efron, 2004]. To illustrate, we assume that the observations are suitably defined difference scores z_i, $i = 1, \ldots, n$ over a large number of distinct hypotheses. The two-group model assumes that the z_i's are drawn either from a null (f_0) or a non-null (f_1) distribution, i.e., each score is drawn from a mixture,

$$z_i \sim f = (1 - \rho) f_0 + \rho f_1, \tag{1}$$

for some weight $\rho \in (0, 1)$, and some probability (density) functions f_0 and f_1. The null component is typically assumed standard normal; however, the true null distribution may differ from the theoretical null, e.g., due to limited sample size or unaccounted correlation. Thus, Efron proposes the estimation of an "empirical null" distribution to adequately capture the range of parameter values coherent with the null hypothesis and accordingly evaluate each testing decision.

In Bayesian nonparametrics, the Dirichlet process (DP) has been extensively used to provide flexible estimates of f_0, or f_1, or both, as well as for clustering the z_i's into common "expression" levels [Do et al., 2005, Dahl and Newton, 2007, Kim et al., 2009, Kottas and Fellingham, 2012]. Martin and Tokdar [2012] develop a flexible hierarchical nonparametric approach where f_0 is assigned a Normal distribution with unknown mean and variance, whereas f_1 is a location mixture of normals. One appealing feature of the two-group model is that the resulting inference is immediately amenable to interpretation in a decision theoretic framework. For example, Efron [2004] describes a local version of the

false discovery rate (*local fdr*), which represents the posterior probability that a difference score z_i is generated according to the null hypothesis, $fdr(z_i) = (1-\rho)\, f_0(z_i)/f(z_i)$. The selection of interesting scores is conducted by flagging all z_i's such that $fdr(z_i) < \alpha$, $\alpha \in (0,1)$, allowing control of the Benjamini–Hochberg FDR [Benjamini and Hochberg, 1995] at level α. More generally, the decision problem could minimize loss functions that compound expected false positive and false negative decisions. The optimal decision would then lead to thresholding the posterior probability of the alternative [e.g., see Muller et al., 2006].

In this manuscript, we investigate the use of a mixture prior of two–parameter Poisson–Dirichlet (2PPD) processes in lieu of the commonly used DPs. The 2PPD process, also known as the *Pitman-Yor* process, is a generalization of the DP and is characterized by two parameters: a "concentration" parameter θ (analogous to the single parameter of the DP), and a "discount" parameter σ. The additional parameter allows for more flexible clustering behavior than the DP and can be used to tune the reinforcement mechanism of large clusters [Lijoi et al., 2007]. We show how the proper choice of σ can be used to model the empirical null distribution f_0 and the uncertainty related to the non-null distribution in the two-group model, leading to improved testing procedures. Our modeling framework further employs non-local prior densities for the base measure of the random probability measures under the alternative hypothesis to allow better separation between the two mixture components. We derive the expression of the exchangeable partition probability function (EPPF), induced by the proposed two-group 2PPD mixture process and observe that, conditional on the assignment of the observations to the null or the alternative hypothesis, the respective random partitions are independent. This property conveniently facilitates posterior inference obtained via MCMC algorithms, which take into account the conditional independence of the partitions. By means of a simulation study, we discuss the performance of our method with respect to the commonly used mixture of DPs and existing state-of-the-art approaches for large-scale multiple comparison problems. We also illustrate the use of the proposed 2PPD processes mixture model on two publicly available datasets: a well-known Prostate cancer dataset [Singh et al., 2002] and one collected from a recent microbiome study [Pop et al., 2014]. In the latter case, the aim was to characterize the microbial composition of the gastrointestinal tracts of children from underdeveloped countries who have been diagnosed with moderate to severe diarrhea. Our study suggests that mixture of DPs should be used with some caution in large scale multiple-testing, and that the use of 2PPD processes could lead to improved operating characteristics.

2 A review of the 2PPD process

In this Section we provide an overview of the 2PPD process with particular regard to its use for density estimation and its clustering properties. Let $Z_1, \ldots, Z_n$ be a sample of n data measurements (e.g. raw observations or summary statistics), drawn from a sequence of exchangeable random elements $Z_1, Z_2, \ldots$, taking value in a complete and separable metric space $\mathbb{Z}$ endowed with its Borel σ-algebra $\mathscr{Z}$. By virtue of the de Finetti

representation theorem,

$$\begin{aligned} Z_i \mid \tilde{p} &\overset{\text{iid}}{\sim} \tilde{p} \qquad i = 1, \ldots, n, \\ \tilde{p} &\sim Q, \end{aligned} \tag{2}$$

for any $n \geq 1$, and for $\tilde{p}$, a random probability measure, with distribution Q defined on the space $\mathscr{P}(\mathbb{Z})$ of probability measures on $\mathbb{Z}$. In a Bayesian framework, Q represents the prior distribution and the model is said to be parametric whenever Q degenerates on a finite dimensional subspace of $\mathscr{P}(\mathbb{Z})$; otherwise, the model is denoted as nonparametric.

Here, we consider the 2PPD process for the random probability measure $\tilde{p}$, which can be represented almost surely as an infinite mixture, i.e., $\tilde{p} = \sum_{k=1}^{\infty} \tilde{w}_k \, \delta_{Y_k}$, where δ_c denotes the point mass at c, the $\tilde{w}_k$'s are random weights obtained as $\tilde{w}_1 = V_1$ and $\tilde{w}_k = V_k \prod_{j=1}^{k-1} (1 - V_j)$, $k \geq 2$ with $V_j \overset{ind}{\sim} \text{Beta}(1 - \sigma, \theta + j\sigma)$, $j \geq 1$ [*stick-breaking construction;* Pitman, 1995], for some $\sigma \in [0, 1)$ and $\theta > -\sigma$. The Y_k's are random locations in $\mathbb{Z}$, independent of the weights $\tilde{w}_k$'s, and assumed as random draws from a non-atomic *base measure* P^*, i.e., $Y_k \overset{\text{iid}}{\sim} P^*$, $k \geq 1$, which represents the prior expected value of the random distribution $\tilde{p}$, i.e., $\mathbb{E}[\tilde{p}(A)] = P^*(A)$ for any $A \in \mathscr{X}$. We should note that the 2PPD process is also well defined for $\sigma < 0$ and $\theta = r|\sigma|$, with r being an integer; however, in such case the process reduces to the parametric Fisher model [Ghosal and van der Vaart, 2017]. Hereafter, we will use $Z_i \mid \tilde{p} \overset{\text{iid}}{\sim} \tilde{p}$, with $\tilde{p} \overset{d}{=} \text{2PPD}(\sigma, \theta, P^*)$, $i = 1, \ldots, n$ to indicate a sample from a 2PPD with parameters σ and θ, and base measure P^*. If $Z_1, \ldots, Z_n$ is a realization from an exchangeable sequence driven by a 2PPD process, there is a positive probability of ties, i.e., $\mathbb{P}[Z_i = Z_j] > 0$ for any $i \neq j$. This *clustering* property often motivates the use of the 2PPD process in statistical applications, e.g. to model data from heterogeneous populations.

The clustering behavior of the 2PPD process can also be investigated by considering the exchangeable partition probability function (EPPF), which characterizes the probability that $Z_1, \ldots, Z_n$ are partitioned into K distinct clusters with respective sizes $n_1, \ldots, n_K$. For the 2PPD process, such probability is $\Pi_K^{(n)}(n_1, \ldots, n_K) = \frac{\prod_{j=1}^{K-1}(\theta + j\sigma)}{(\theta+1)_{n-1}} \prod_{j=1}^{K} (1 - \sigma)_{n_j - 1}$ for any choice of positive integers $n_1, \ldots, n_K$ such that $\sum_{i=1}^{K} n_i = n$, with $K \in \{1, \ldots, n\}$ and $(a)_q = \Gamma(a+q)/\Gamma(a)$, for any non-negative integer q. The expression highlights how the values of the parameters σ and θ affect the clustering structure induced by the 2PPD process. It is well-known that if K_n denotes the number of distinct values recorded in a sample $Z_1, \ldots, Z_n$ of an exchangeable sequence drawn according to a 2PPD(σ, θ) process, then $K_n / n^{\sigma} \to S_{\sigma,\theta}$ as $n \to \infty$ (almost surely) for some positive random variable $S_{\sigma,\theta}$ when $\sigma \in (0, 1)$[see Theorem 3.8 in Pitman, 2002]. When $\sigma = 0$, we recover the clustering behavior of the Dirichlet process, obtaining $K_n / \log n \to \theta$ as $n \to \infty$ (almost surely). Hence, the larger σ is, the larger the number of clusters. Moreover, σ controls the reinforcement of the partition, i.e., the ability of big clusters to attract even more observations, as highlighted by the predictive distribution of the

2PPD process,

$$\mathbb{P}[Z_{n+1} \in A \mid Z_1, \ldots, Z_n] = \frac{\theta + \sigma\, K_n}{\theta + n - 1}\, P^* + \sum_{j=1}^{K_n} \frac{n_j - \sigma}{\theta + n - 1}\, \delta_{Z_j^*}(A),$$

where the probability that a new observation is assigned to an existing cluster, and assumes value Z_j^*, $j = 1, \ldots, K_n$, is proportional to $n_j - \sigma$. Therefore, values of σ close to 1 favor the formation of a large number of clusters, most of which are singletons [Lijoi et al., 2007].

Finally, we consider the variability of realizations from a 2PPD process around the base measure P^*. The variance of the process is $\mathrm{Var}[\tilde{p}(A)] = \frac{1-\sigma}{\theta+1}\, P^*(A)[1 - P^*(A)]$, for any $A \in \mathscr{X}$ and $j = 0, 1$. Large values of σ correspond to random probability measures which are more concentrated around the base measure P^*. Therefore, one should expect that the empirical distribution function of any sample $Z_1, \ldots, Z_n$ drawn from a 2PPD process with high values of σ, $F_n(b) = \tilde{p}(\infty, b] = \sum_{k=1}^{\infty} \tilde{w}_k\, \delta_{Z_k^*}(\infty, b]$, would be characterized by a large number of weights $\tilde{w}_k$ of similar size. In the next Sections we will exploit these properties to guide the use of the 2PPD process in the two-group model for multiple testing.

3 Methods

3.1 A two-group 2PPD model

The different clustering behavior that the 2PPD process exhibits as a function of σ can be exploited for distinguishing between the null and alternative distributions in the two-group model. More precisely, we first rewrite model (2) as the two–component mixture,

$$\tilde{p} = (1 - \rho)\, \tilde{p}_0 + \rho\, \tilde{p}_1, \tag{3}$$

where $\tilde{p}_j \sim \mathrm{2PPD}(\sigma_j, \theta_j, P_j^*)$ represents the unknown distribution under the null and the alternative hypotheses, for $j = 0$ and $j = 1$, respectively. Similarly as in (1), the mixture weight ρ is a random variable independent of the $\tilde{p}_j$'s and takes values in $[0, 1]$. We further introduce an auxiliary binary random variable γ_i, $i = 1, \ldots, n$, such that $Z_i \sim \tilde{p}_0$ if $\gamma_i = 0$ and $Z_i \sim \tilde{p}_1$ if $\gamma_i = 1$. Thus, conditionally on the $\gamma_i's$, we can rewrite (2)–(3) as

$$\begin{aligned} Z_i \mid \gamma_i &\overset{\text{ind}}{\sim} \tilde{p}_{\gamma_i}, \qquad i = 1, \ldots, n, \\ \gamma_i \mid \rho &\overset{\text{iid}}{\sim} \text{Bernoulli}(\rho), \\ \tilde{p}_{\gamma_i} &\sim \mathrm{2PPD}(\sigma_{\gamma_i}, \theta_{\gamma_i}, P_{\gamma_i}^*), \end{aligned} \tag{4}$$

with $\tilde{p}_0$ and $\tilde{p}_1$ independent, and assuming a $\mathrm{Beta}(a, b)$ distribution on ρ. The hyperparameters a and b influence the proportion of discoveries and can be tuned according to the problem at hand. In genomic studies, one may want to enforce sparsity of discoveries, with prior expected proportions $\mathbb{E}[\rho] = \frac{a}{a+b}$ between 1% and 10% of the total number

of hypotheses. A lower value of $\mathbb{E}[\rho]$ typically results in lower posterior probabilities of the alternative, although the relative ranking of the posterior probabilities is overall preserved.

We exploit the properties of the 2PPD process discussed in Section 2 and propose to specify the hyperparameters of the null and non-null random probability measures in (4) as follows. In accordance with Efron's idea that the empirical null distribution should capture only small departures from the theoretical null, we let $\tilde{p}_0$ concentrate around the theoretical null. Furthermore, we assume that there's no good model *a priori* for the non-null distribution. Therefore, $\tilde{p}_1$ is allowed to vary more freely on the space of the alternative distributions. Under the null distribution, the process should encourage the creation of a large number of clusters each composed by few observations, so that the empirical distribution well approximates the theoretical null. For the non-null distribution, we should expect a more uneven distribution of the realizations. Based on those considerations, we propose to set $\sigma_0 > \sigma_1$. We will discuss how such a choice might help discriminating between the null and the alternative distribution in the multi-comparison problem.

We conclude this Section by considering the joint partition structure induced by model (4) for a sample $Z_1, \ldots, Z_n \mid \tilde{p} \overset{\text{iid}}{\sim} \tilde{p}$. Let $\Pi^{(n)}_{K,j}(n_1, \ldots, n_K)$ denote the EPPF of process $\tilde{p}_j$, $j = 0, 1$, that is the probability that n observations are assigned to K different clusters of sizes $(n_1, \ldots, n_K)$. For notational simplicity, we assume that $\Pi^{(n)}_{K+1,j}(n_1, ..., n_K, 0) \equiv \Pi^{(n)}_{K,j}(n_1, \ldots, n_K)$, for any $j = 0, 1$ and $n_1, \ldots, n_K \geq 1$ such that $\sum_{i=1}^{K} n_i = n$. Then the following result provides the EPPF of the mixture of 2PPD processes as below:

PROPOSITION 1. *The EPPF associated to the mixture of 2PPD processes in* (4) *is given by:*

$$\Pi^{(n)}_K(n_1, \ldots, n_K) = \frac{1}{(a+b)_n} \sum_{\boldsymbol{i} \in \times_{j=1}^{K} \{0, n_j\}} (a)_{|\boldsymbol{i}|} (b)_{n-|\boldsymbol{i}|} \times \Pi^{(|\boldsymbol{i}|)}_{K_0,0}(i_1, \ldots, i_K)\, \Pi^{(n-|\boldsymbol{i}|)}_{K_1,1}(n_1 - i_1, \ldots, n_K - i_K) \quad (5)$$

where $\boldsymbol{i} = (i_1, \ldots, i_K)$, $|\boldsymbol{i}| = i_1 + \cdots + i_K$, $K_0 = card\{j : i_j = n_j\}$ *and* $K_1 = K - K_0$. *If* $i_k = n_k$ *or* $i_k = 0\ \forall k$, *we assume* $\Pi^{(n)}_K(i_1, \ldots, i_K) = 1$.

See Web Appendix B for a proof. Direct use of (5) is far from trivial. Nonetheless, the expression lends itself to an interesting interpretation: conditional on the assignment of the clusters to either $\tilde{p}_0$ or $\tilde{p}_1$, the respective random partitions are still independent. This remark is useful for devising a suitable computational algorithm for posterior inference.

3.2 Bayesian hierarchical two-group mixture model

In many applications, the discreteness of the realizations of the 2PPD process may be considered inadequate. Thus, in lieu of (4), it is often common to assume for a sample

$Z_1, \ldots, Z_n$ a hierarchical mixture model with continuous components, i.e.

$$Z_i|\tilde{p} \overset{\text{iid}}{\sim} \tilde{p}, \quad \text{with} \quad \tilde{p} = (1-\rho) \int k_0(Z_i, \vartheta)\, \tilde{p}_0(d\vartheta) + \rho \int k_1(Z_i, \vartheta)\, \tilde{p}_1(d\vartheta), \tag{6}$$

that is the two-group model is characterized by a null and non-null distributions which are each defined as a 2PPD process mixture. Here, $f_{\tilde{p}}(Z_i)$ is the random density induced by the random probability measure $\tilde{p}$, while $k_j : \mathbb{Z} \times \Theta \to \mathbb{R}^+$, $j = 0, 1$ are general kernels such that for $\boldsymbol{\vartheta} \in \Theta$ and some σ–finite measure λ on $(\mathbb{Z}, \mathscr{Z})$ one has $\int_{\mathbb{Z}} k_j(x, \boldsymbol{\vartheta})\, \lambda(\mathrm{d}x) = 1$, $j = 0, 1$. For our purposes, it is convenient to set $\mathbb{Z} = \mathbb{R}$ and let λ coincide with the Lebesgue measure on $\mathbb{R}$ so that the previous model defines a prior on the space of density functions on $\mathbb{R}$. By conditioning on the auxiliary group indicator variables γ_i, $i = 1, \ldots, n$, we can rewrite model (6) as a hierarchical Bayes *two-group 2PPD process mixture*,

$$\begin{aligned}
Z_i \mid \boldsymbol{\vartheta_i}, \gamma_i &\overset{\text{ind}}{\sim} k_{\gamma_i}(Z_i \mid \boldsymbol{\vartheta}_i), \qquad i = 1, \ldots, n \\
\boldsymbol{\vartheta}_i \mid \gamma_i, \tilde{p} &\overset{\text{ind}}{\sim} \tilde{p}_{\gamma_i}, \\
\gamma_i \mid \rho &\overset{\text{iid}}{\sim} \text{Bernoulli}(\rho), \\
\rho &\sim \text{Beta}(a, b) \\
\tilde{p}_{\gamma_i} &\sim \text{2PPD}(\sigma_{\gamma_i}, \theta_{\gamma_i}, P^*_{\gamma_i}),
\end{aligned} \tag{7}$$

where $\boldsymbol{\vartheta}_i$ may indicate either a scalar or a vector parameter. In general, $k_0(\cdot)$ and $k_1(\cdot)$ could be different. Here, we assume $k_{\gamma_0}(\cdot) = k_{\gamma_1}(\cdot) = k(\cdot)$ to be a Normal kernel and set $\boldsymbol{\vartheta_i} = (\mu_i, \tau_i^2)$. For notational simplicity, in (7) we have omitted additional hyperparameters which may feature in the kernel function $k(\cdot)$ but are not relevant for the decision problem and thus are assigned separate priors.

We conclude the specification of the two-group model (7) by discussing the choice of the base measures P_0^* and P_1^*. On the one hand, we achieve flexible estimation of the so-called "empirical null" distribution by setting $P_0^*\left(\mu, \tau^2\right) = \pi\left(\mu\right) \times \pi\left(\tau^2\right) = \mathcal{N}\left(0, 1\right) \times IG\left(a_0, b_0\right)$. where the parameters of the IG on τ^2 are chosen so to allow relatively small deviations from the theoretical null distribution. For example, by assuming $a_0 = 5$, $b_0 = 0.2$, the induced marginal distribution on Z_i has only slightly fatter tails than the standard normal.

Moreover, P_0^* and P_1^* should not have significantly overlapping supports, i.e. they should assign high probability to regions of the parameter space that are consistent with the null and the alternative hypotheses, respectively. In the Bayesian multiple hypotheses testing framework, this requirement has sometimes been advocated to ensure enough *separation* between the null and the alternative models. Thus, we first model P_1^* as a symmetric bimodal mixture of Normal-Inverse Gamma (NIG) distributions, as $P_1^* = \frac{1}{2}\text{NIG}(-|m_1|, k_1, \alpha_1, \beta_1) + \frac{1}{2}\text{NIG}(|m_1|, k_1, \alpha_1, \beta_1)$, with $m_1 \in \mathbb{R}$, and $k_1, \alpha_1, \beta_1 \in \mathbb{R}^+$. Marginally,

$$\pi\left(\mu_1|m_1\right) = \frac{1}{2}\left[\sqrt{\frac{\beta_1}{\alpha_1}} t_{2\alpha_1} - |m_1|\right] + \frac{1}{2}\left[\sqrt{\frac{\beta_1}{\alpha_1}} t_{2\alpha_1} + |m_1|\right].$$

We further achieve separation in the multiple hypotheses testing problem by modeling the location parameter m_1 with a non-local prior (NLP), i.e. a prior that assigns vanishing density to small neighborhoods of the null hypothesis [Johnson and Rossell, 2010]. Several types of NLP have been proposed in the literature. See, for instance, Rossell and Telesca [2017]. Here, we adopt an r-th moment (MOM) prior for m_1, with

$$\pi_{MOM}\left(m_1; 0, \kappa^2, r\right) = \frac{m_1^{2r}}{\xi} \frac{e^{-m_1^2/2\kappa^2}}{\sqrt{2\pi\kappa^2}}, \tag{8}$$

where ξ is the normalizing constant, and we write $m_1 \sim NLP_{MOM}\left(0, \kappa^2, r\right)$. Specific hyper-parameter specifications will be detailed in Section 4. Here, we only note that the non-local prior specification in P_1^* should provide enough separation from the origin to ensure good estimation of the posterior probability of the alternative. Finally, the other parameters of the 2PPD processes are set such that $\theta_0 = \theta_1$ and $\sigma_0 > \sigma_1$. In general, θ_0 and θ_1 are chosen relatively small, in order to enforce coarser clustering structures, especially under the alternative hypothesis. Typically, in Dirichlet-Process two-groups models, $\theta_0 = \theta_1 = 1$ [see, e.g. Do et al., 2005]. From the discussion at the end of Section 2, it follows that realizations of the 2PPD null process are expected to be more concentrated around the base measure. In the next Sections we will investigate the effect of different choices for the parameter values of the 2PPD processes for the multiple comparison problem.

3.3 Posterior inference

Posterior inference for model (4) or (7) relies on Markov Chain Monte Carlo techniques since the posterior distributions are not available in closed form. Our primary interest is in the group indicators γ_i's, which uniquely identify the random probability measure from which the data Z_i's were generated, and, correspondingly, the probability of group membership, ρ. For the sampling of the γ_i's, we exploit the independence of the random partitions implied by the EPPF (5) of the proposed mixture of 2PPD processes. More specifically, if $Z_1, \ldots, Z_n$ are a random sample from (4) and P_j^*, $j = 0, 1$ are non-atomic base measures with common support, then $\mathbb{P}[Z_i = Z_j \mid \gamma_i \neq \gamma_j] = 0$ for $i \neq j$. Thus, all the Z_i's in a cluster are generated by the same 2PPD process. The details of the MCMC algorithms are provided in the Web Appendix A. In particular, we employ a split-merge move to speed up computations for large sample sizes [Dahl, 2005]. The computational burden of the MCMC algorithm increases for higher values of either θ_0, θ_1, σ_0 or σ_1 due to the increased number of latent clusters generated by the 2PPD process. A discussion of the computational efficiency of a plain Pólya-Urn sampler versus the split-merge implementation is also provided in the Web Appendix D.

Posterior inference on the weight ρ in (4) is conducted by means of post-MCMC analysis, by approximating the posterior expected value $\mathbb{E}[\rho \mid \text{data}]$ using auxiliary indicators, say $\boldsymbol{\gamma}_t^* = (\gamma_{1,t}^*, \ldots, \gamma_{K^{(t)},t}^*)$, which denote if cluster $k \in 1, \ldots K^{(t)}$ at iteration $t = 1, \ldots, T$ is a realization from $\tilde{p}_0$ or $\tilde{p}_1$. More precisely, if we denote by $B < T$ the burn-in period of the chain, we can compute the following Monte Carlo approximation

of the posterior expected value $\mathbb{E}[\rho \mid \text{data}] \approx \frac{1}{T-B}\sum_{t=B+1}^{T} \frac{a+\sum_{k=1}^{K^{(t)}} n_{k,t}(1-\gamma^*_{k,t})}{a+b+n}$.

Similarly, the posterior probability that an observation belongs to the non-null group can be obtained from the MCMC output as $PP_i^1 = p(\gamma_i = 1 \mid \text{data}) \approx \frac{1}{T-B}\sum_{t=B+1}^{T}\gamma_{i,t}$, where the $\gamma_{i,t}$'s indicate the MCMC draws of the component indicators γ_i's. Then, a score Z_i is considered significant if the corresponding PP_i^1 is larger than a threshold, say κ, chosen to control the Bayesian FDR at a pre-assigned $\alpha \times 100\%$ level , $BFDR(\kappa) = \frac{\sum_{\nu=1}^{V}(1-\text{PP}_\text{i}^1)I(\text{PP}_\text{i}^1>\kappa)}{\sum_{\nu=1}^{V} I(\text{PP}_\text{i}^1>\kappa)} < \alpha$ [Newton et al., 2004, Muller et al., 2006].

4 Applications

4.1 Simulation study

We investigate the performance of the Bayesian hierarchical 2PPD mixture modeling framework described in (6)–(7) for large-scale multiple hypothesis testing by means of a simulation study under $S = 5$ scenarios. More specifically, we simulate z-scores from mixture (1), where $f_0(z) = \mathcal{N}(z \mid 0, \sigma_s^2)$. We set $\sigma_s^2 = 1$ for $s = 1, \ldots 4$. For the fifth scenario, we set $\sigma_5^2 = 1.5$ to model the effect of hidden correlation among observations and of the association with unobserved covariates, that may lead to departures from standard Gaussianity. For f_1 we choose:

- **Scenario 1**: $f_1(z) = 0.67 \cdot \mathcal{N}(z| -3, 2) + 0.33 \cdot \mathcal{N}(z|3, 2)$,
- **Scenario 2**: $f_1(z) = \mathcal{N}(z \mid u, 1)$ with $u \sim \text{Uniform}(2, 4)$,
- **Scenario 3**: $f_1(z) = \mathcal{N}(z \mid u, 1)$ with $u \sim \text{Uniform}([-4, -2] \cup [2, 4])$,
- **Scenario 4**: $f_1(z) = \text{Gamma}((-1)^v \cdot z \mid a, b)$ with $a = 4$, $b = 1$ and $v \sim \text{Bernoulli}(0.5)$,
- **Scenario 5**: $f_1(z) = 0.5 \cdot \mathcal{N}(z|5, 1) + 0.5 \cdot \mathcal{N}(z| -5, 1)$,

i.e. f_1 is assumed asymmetric unimodal (scenario 1), symmetric bimodal (scenarios 2), asymmetric bimodal (scenario 3) and symmetric bimodal with fat tails (scenario 4 and scenario 5), thus mimicking typical high-dimensional testing situations. An illustrative plot of data generated under the five scenarios is provided in the Web Appendix C. In all scenarios, we set $\rho = 0.05$, since typically only a small proportion of the comparisons is expected to be significant in large-scale inference hypothesis testing. Each simulation includes $n = 1,000$ simulated scores and is replicated 30 times to allow quantification of posterior uncertainty and of the frequentist operating characteristics of the testing procedures.

For model fitting, we employ the mixture model (6)–(7), where we assume $k(\cdot \mid \theta_i) = \text{Normal}(\cdot \mid \boldsymbol{\vartheta}_i)$, with $\boldsymbol{\vartheta}_i = (\mu_i, \tau_i^2)$. The base measure of the 2PPD process $\tilde{p}_0$ is chosen as described in Section 3.2, with $a_0 = 5$, $b_0 = 0.2$. For P_1^*, we set $k_1 = 1/3$, $\alpha_1 = 1$, $\beta_1 = 1$. A NLP_{MOM} prior is assumed for m_1, with $r = 3$ and $\kappa = 2$. For the parameters

characterizing the clustering behavior of the 2PPD process priors, we investigate the effect of different choices of (σ_0, σ_1) on the inference, with $\sigma_0 > \sigma_1$. More specifically, here we report the inference for the following values for the pair (σ_0, σ_1): $(0.75, 0)$, which corresponds to assuming a DP on the non-null component; in addition to $(0.75, 0.1)$, $(0.75, 0.25)$, $(0.9, 0.25)$ to investigate the effect of decreased prior uncertainty, $Var(\tilde{p})$, on the components of the two-group 2PPD mixture. We further set the concentration parameters $\theta_0 = \theta_1 = 1$ [Do et al., 2005]. For the Beta prior on ρ, we set $a = 1$ and $b = 9$. For each dataset, the MCMC algorithm was run for 2,500 iterations after a 2,500 iterations burn-in period. The evaluation of posterior convergence was conducted using standard Bayesian convergence diagnostics on the chains of the traceable parameters, m_1 and ρ, by monitoring the number of group components and by inspecting the estimated densities of the null and non-null processes.

We compare the performance of our modeling approach with five alternative methods for large-scale hypothesis testing: (a) a two-group DP mixture model, which can be seen as a special case of the modeling framework proposed here, obtained by setting $\sigma_0 = \sigma_1 = 0$, with a non-local prior on the base measure for the alternative distribution (b) the local false discovery rate of Efron [2004]; (c) the Benjamini and Hochberg procedure [BH, Benjamini and Hochberg, 1995]; (d) the empirical Bayes mixture model of Muralidharan [2012], which allows simultaneous estimation of the effect size and of the local false discovery rate, and (e) the empirical Bayes semi-parametric approach of Martin and Tokdar [2012].

For each simulation replicate, results were compared using several performance measures: the Matthews Correlation Coefficient (MCC), which can be computed from a confusion matrix as $\text{MCC} = (TP \times TN - FP \times FN)/\sqrt{(TP+FP)(TP+FN)(TN+FP)(TN+FN)}$, where TP, TN, FP, and FN are the number of true positive, true negative, false positive and false negative results, respectively; the F1 score, $2\text{TP}/(2\text{TP} + \text{FP} + \text{FN})$; as well as precision, specificity, accuracy and the area under the curve (AUC) of the corresponding receiver operating characteristic curve. For each simulation, we identify significant scores by controlling the Bayesian false discovery rate [Newton et al., 2004], the local false discovery rate [Efron, 2004] and the frequentist false discovery rate [Benjamini and Hochberg, 1995] at the 10% level.

In Table 1 we report the performance metrics achieved in the different simulation scenarios as a function of the combinations of hyperparameters of the 2PPD process. Overall, the performance of the proposed 2PPD process is similar, as long as $\sigma_1 < \sigma_0$. Higher values of σ_0 lead to draw samples from f_0 which are closer to the theoretical null, but the implied tighter control of the variance of the null process may lead to a slightly decreased performance in some scenarios. If $\sigma_1 > \sigma_0$, the performance can deteriorate considerably.

Table 2 reports the results from the comparison with alternative multiple testing methods. Compared to our method, the method of Martin and Tokdar [2012] performs quite well in all scenarios except the fat-tailed one, Scenario 4, where our 2PPD model outperforms four out of five competitors. The BH procedure also performs quite well, although

with slightly lower precision, in the first four scenarios. However, small departures from the standard Gaussian null assumption (scenario 5) considerably affect the performance of the BH procedure. The performance of two-group DP mixtures is impacted by the flexible modeling of both the null and alternative distribution, which leads to a relatively high number of false assignments. This result is remarkable as various types of mixture of DP processes have been often proposed for hypothesis testing in the two-group modeling framework. The results also appear fairly robust to different sample sizes (see Web Appendix E).

4.2 Case study: Microbiome data

We illustrate the applicability of the proposed two-group 2PPD process model on a publicly available dataset of microbial abundances from a case-controlled study on post-diarrheal disruption in children from low-income countries. The purpose of the study was to identify potential microbiota which may show positive associations with moderate-to-severe diarrhea (MSD) in the case group. Negative associations are also of interest since they may suggest potential target treatments for recovery from dysbiosis.

Stool samples were obtained from 992 children between the ages of 0 and 59 months, 508 of whom had recently suffered from moderate to severe diarrhea, with the remaining 484 children acting as age-matched controls. The samples were obtained in Mali (M), the Gambia (G), Kenya (K), and Bangladesh (B) and case/control proportions were approximately equal for each country.

Due to the nature of the sampling mechanism, the distribution of the microbiome counts is highly skewed, i.e., a few are highly abundant, whereas most microbes have low frequencies [Chen and Li, 2016]. Here, we are interested in evaluating the ability of our model to identify microbiota which may be differently abundant in healthy and MSD subjects. Therefore, we employ a Negative-Binomial regression model on the taxonomic abundances y_{ij}, where $j = 1, \ldots, J_i$ indexes the microbiotic taxa, and $i = 1, \ldots, n$ indexes the samples. As it is typical when dealing with sequencing data [see, e.g., Witten, 2011], we let s_i denote an estimate of a sample-specific size factor, to take into account the different sequencing depths of the samples. Also, we let x_{ij}^{case}, x_{ij}^{age} and $x_{ij}^{country}$ denote the three available covariates for the MSD status, age and country. More specifically, $x_{ij}^{case} = 1$ for cases and $x_{ij}^{case} = 0$ for the matched controls. We adopt Gambia as the reference value for the other countries, and let x_{ij}^{K}, x_{ij}^{B}, and x_{ij}^{M} be dummy variables for the other countries. Then, we assume:

$$
\begin{aligned}
y_{ij} &\overset{\text{ind}}{\sim} NB(\mu_{ij}, \alpha_j), \qquad j = 1, \ldots, J_i;\ i = 1, \ldots, n, \\
\log(\mu_{ij}) &= \log(s_i) + \beta_{0,j} + \beta_{1,j}\, x_{ij}^{case} + \beta_{2,j}\, x_{ij}^{age} + \beta_{3,j}\, x_{ij}^{M} + \beta_{4,j}\, x_{ij}^{B} + \beta_{5,j}\, x_{ij}^{K} + \epsilon_{ij},
\end{aligned}
$$

where α_j represents a taxon-specific dispersion parameter, and $\beta_{0,j}$ represents a taxon-specific effect, which captures the abundance of taxon j in the control group, and the $\beta_{k,j}$'s represent the effects of each covariate on the taxon abundance. The Negative Binomial distribution was chosen due to its flexibility over the Poisson alternative. The model was fitted using the `glmmTMB` package. To illustrate our multiple testing procedure, we

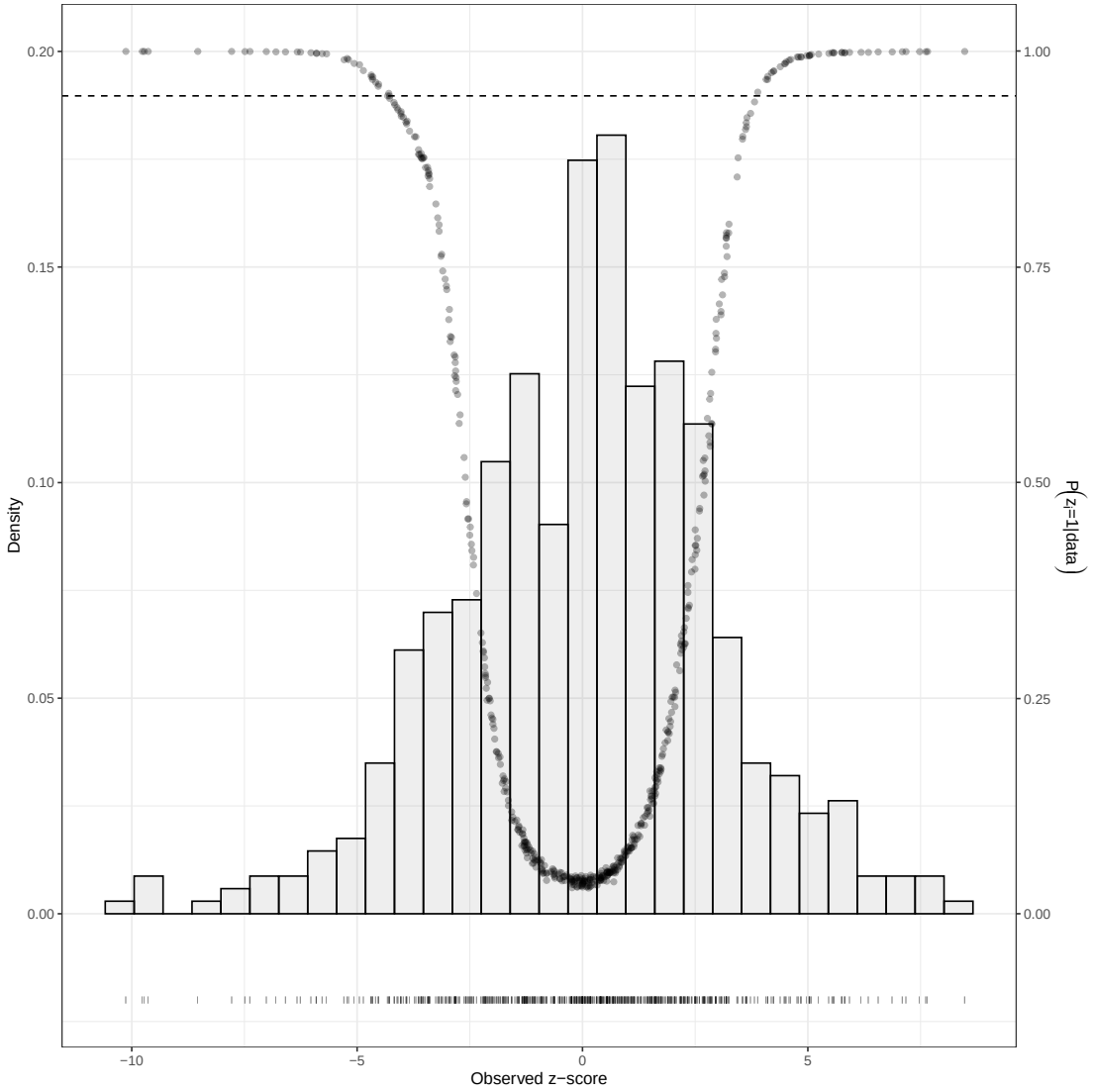

Figure 1: Microbiome data case study: Histogram of 535 z-scores obtained from the case term (β_1) in the Negative Binomial generalized linear mixed effects model. We superimpose the posterior probabilities of the events $\{\gamma_i = 1|\boldsymbol{z}\}$ and the threshold corresponding to a Bayesian FDR of 1%.

consider the fixed case-control effect captured by the estimates of the coefficients $\beta_{1,j}$'s, which provide the z-scores for testing the differences in abundance between healthy and MSD subjects. A histogram of the 535 z-scores from the data is given in Figure 1. Since the estimated coefficients are a function of the original data, the independence assumption may not be satisfied if the original taxonomic abundances are correlated. Indeed, the presence of hidden correlation among the observables and unknown associations

with unobserved covariates are major motivations for the two-group model formulation in Efron [2004].

In the two-group model (6)–(7), we fix the hyperparameters for the prior processes as $\theta_0 = \theta_1 = 1$, $\sigma_0 = 0.75$, $\sigma_1 = 0.10$. The specific choice for σ_0 allows small departures of the empirical null from the theoretical $\mathcal{N}(0, 1)$ distribution, while maintaining computational feasibility in the generation of the latent clusters from the null. A Beta$(1, 99)$ is chosen for ρ to further encourage sparsity of discoveries. The hyperparameters of the base measures were set as in Section 4.1. For the results provided here, we run 20,000 iterations after 20,000 iterations as burn-in. Figure 1 overlays the Monte Carlo estimates of the posterior probability of each taxon belonging to the non-null distribution to the histogram of the z-scores. By thresholding the Monte Carlo estimate of posterior probability of the non-null process at a value corresponding to a Bayesian false discovery rate [Newton et al., 2004] of 1%, we identify a total of 74 non-null taxa. On the contrary, the BH procedure leads to 143 significant microbes, when controlling the FDR at the 1% level. The *locfdr* model detects as relevant only 6 taxa. Tables 1 and 2 in the Web Appendix F report the taxa with the highest discovery probabilities, separately for positive and negative z-scores. A close inspection of our results reveals some interesting biological findings (see Web Appendix G).

4.3 Case study: Prostate Cancer Dataset

To assess how our model performs in large-sample cases, we apply our methodology to the widely known *Prostate* dataset of Singh et al. [2002]. See also Efron [2009]. We exploit the split-merge move in the MCMC to improve computational efficiency (see Web Appendix D). The dataset is composed of 6,033 genes for 102 observations from 52 prostate cancer patients and 50 healthy men. We adopt the same prior specification as in the microbiome case study, with the exception that here we set $b = 9$, as in the simulation studies. This choice is in accordance with the discussion in Efron [2008], who suggests a proportion *a priori* of no more than 10% non-null genes for these data. Figure 2 reports the posterior probabilities of discovery for this dataset. When thresholding the BFDR at the 20% level, our method flags only 18 genes as relevant. Similarly, the *locfdr* procedure flags 19 genes. On the contrary, the BH procedure identifies 60 genes as significant, even when thresholding the FDR at the 10% level.

5 Discussion and Conclusion

We have considered the two-group model by Efron [2004] for multiple hypotheses testing and we have proposed the use of a mixture prior of two–parameter Poisson–Dirichlet processes as a flexible class of prior processes in that framework. In particular, an appropriate choice of the hyperparameters of the 2PPD processes allows the characterization of small departures from the theoretical null in the estimation of the empirical null distribution, while leaving flexibility in the modeling of the non-null distribution. We have also employed a mixture of non-local prior densities as base measure for the alternative

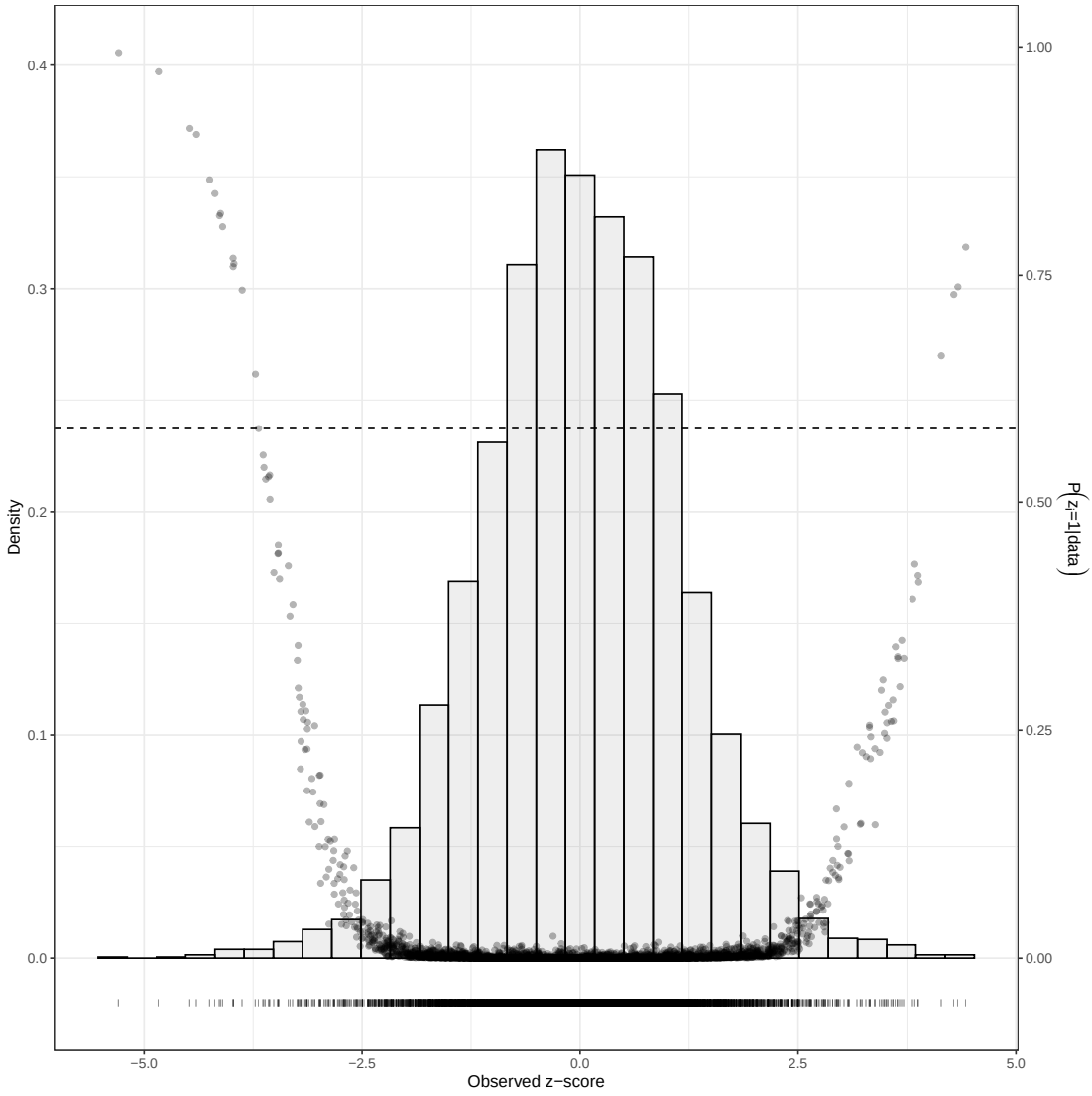

Figure 2: Prostate dataset: Histogram of 6033 z-scores obtained from a two-groups comparison. We superimpose the posterior probabilities of the events $\{\gamma_i = 1|\boldsymbol{z}\}$ and the threshold corresponding to a Bayesian FDR of 20%.

distribution, to improve separation and facilitate the estimation and identifiability of the mixture components. The proposed approach has been shown to provide a robust testing procedure, which compares favorably with recently proposed methods for estimating the components of the two-group model, including the widely-used DP mixture models. A limitation of the procedure is related to the computing effort, since Markov chain Monte Carlo algorithms for Bayesian nonparametric models typically require considerable computational time for posterior inference. To provide an illustration, in the analysis of the Prostate cancer dataset of Section 4.3, it took approximately 56 hours to run 20,000 MCMC iterations on a Xeon(R) E5-2640 v4, 2.40GHz Linux sever, with the computational bottleneck being represented by the iterations requiring a full Pólya-Urn sampling. Variational Bayes techniques have been developed for many Bayesian nonparametric models, including the 2PPD process [see, e.g. Jordan and Blei, 2006]. However, the speed up of MCMC algorithms for Bayesian nonparametric models in high-dimensional settings is still a topic of ongoing research [see, e.g., Canale et al., 2019].

A careful choice of the hyperparameters of the two-group 2PPD model is essential to ensure good operating characteristics of the testing procedures. We have followed prevailing practices and set $\theta_0 = \theta_1 = 1$ in both the simulations and the data analyses. Priors on θ_0 and θ_1 would need to incorporate constraints to facilitate the identification of the two-group components.

Finally, in our data analyses, we have proposed a two-group model for the analysis of data observed under two conditions. However, often the interest is in studying longitudinal changes of repeated measurements within a subject. Therefore, models that take into account the temporal dependence of the hypotheses are required.

Acknowledgements

The authors thank the reviewers and the Editor for their careful and inspiring comments, that helped improving the content and the structure of this article. A. Lijoi has been partially supported by MIUR, grant 2015SNS29B.

Data Availability Statement

The data that support the findings in this paper are openly available in the R packages `msd16s` at `http://doi.org/10.1186/gb-2014-15-6-r76` [Pop et al., 2014] and `sda`, at `https://CRAN.R-project.org/package=sda` [Ahdesmaki et al., 2015].

References

Miika Ahdesmaki, Verena Zuber, Sebastian Gibb, and Korbinian Strimmer. *sda: Shrinkage Discriminant Analysis and CAT Score Variable Selection*, 2015. URL `https://CRAN.R-project.org/package=sda`. R package version 1.3.7.

Yoav Benjamini and Yosef Hochberg. Controlling the False Discovery Rate: a practical and powerful approach to multiple testing. *Journal of the Royal Statistical Society. Series B: Statistical Methodology*, 57(1):289–300, 1995. ISSN 00359246. doi: 10.2307/2346101. URL http://www.stat.purdue.edu/{~}doerge/BIOINFORM.D/FALL06/BenjaminiandYFDR.pdf{%}5Cnhttp://engr.case.edu/ray{_}soumya/mlrg/controlling{_}fdr{_}benjamini95.pdf.

Antonio Canale, Riccardo Corradin, and Bernardo Nipoti. Importance conditional sampling for Bayesian nonparametric mixtures. 2019. URL http://arxiv.org/abs/1906.08147.

Eric Z. Chen and Hongzhe Li. A two-part mixed-effects model for analyzing longitudinal microbiome compositional data. *Bioinformatics*, 32(17):2611–2617, 2016. ISSN 14602059. doi: 10.1093/bioinformatics/btw308.

Y.-Y. Chen, G. D. Wu, M. Bewtra, H. Li, K. Bittinger, K. Gupta, E. Gilroy, J. Chen, R. Sinha, D. Knights, L. Nessel, W. A. Walters, F. D. Bushman, R. Baldassano, R. Knight, S. A. Keilbaugh, J. D. Lewis, and C. Hoffmann. Linking Long-Term Dietary Patterns with Gut Microbial Enterotypes. *Science*, 334(6052):105–108, 2011. ISSN 0036-8075. doi: 10.1126/science.1208344. URL http://www.sciencemag.org/content/334/6052/105.short.

D B Dahl. Sequentially-allocated merge-split sampler for conjugate and nonconjugate Dirichlet process mixture models. *Journal of Computational and Graphical Statistics*, 2005.

David B. Dahl. An improved merge-split sampler for conjugate Dirichlet process mixture models. *Technical Report*, 2003.

David B. Dahl and Michael A. Newton. Multiple hypothesis testing by clustering treatment effects. *Journal of the American Statistical Association*, 102(478):517–526, 2007. ISSN 01621459. doi: 10.1198/016214507000000211. URL http://www.tandfonline.com/doi/abs/10.1198/016214507000000211.

M. Di Paola, G. Pieraccini, D. Cavalieri, P. Lionetti, S. Massart, M. Ramazzotti, J. B. Poullet, S. Collini, and C. De Filippo. Impact of diet in shaping gut microbiota revealed by a comparative study in children from Europe and rural Africa. *Proceedings of the National Academy of Sciences*, 107(33):14691–14696, 2010. ISSN 0027-8424. doi: 10.1073/pnas.1005963107. URL http://www.pubmedcentral.nih.gov/articlerender.fcgi?artid=2930426{&}tool=pmcentrez{&}rendertype=abstract.

Kim Anh Do, Peter Müller, and Feng Tang. A Bayesian mixture model for differential gene expression. *Journal of the Royal Statistical Society. Series C: Applied Statistics*, 54(3):627–644, 2005. ISSN 00359254. doi: 10.1111/j.1467-9876.2005.05593.x. URL http://doi.wiley.com/10.1111/j.1467-9876.2005.05593.x.

Bradley Efron. Large-scale simultaneous hypothesis testing: the choice of a null hypothesis. *Journal of the American Statistical Association*, 99(465):96–104, 2004. ISSN 0162-1459. doi: 10.1198/016214504000000089. URL http://www.tandfonline.com/doi/abs/10.1198/016214504000000089.

Bradley Efron. Microarrays, empirical bayes and the two-groups model. *Statist. Sci.*, 23 (1):1–22, 02 2008. doi: 10.1214/07-STS236.

Bradley Efron. Empirical Bayes estimates for large-scale prediction problems. *Journal of the American Statistical Association*, 104(487):1015–1028, 2009. ISSN 01621459. doi: 10.1198/jasa.2009.tm08523.

Subhashis Ghosal and Aad van der Vaart. *Fundamentals of Nonparametric Bayesian Inference*. Cambridge University Press, 2017.

Hemant Ishwaran and Lancelot F. James. Gibbs sampling methods for stick-breaking priors. *Journal of the American Statistical Association*, 96(453):161–173, 2001. ISSN 1537274X. doi: 10.1198/016214501750332758. URL http://www.tandfonline.com/doi/abs/10.1198/016214501750332758.

Sonia Jain and Radford M. Neal. A Split-Merge Markov Chain Monte Carlo procedure for the Dirichlet process mixture model. *Journal of Computational and Graphical Statistics*, 13(1):158–182, 2004. ISSN 10618600. doi: 10.1198/1061860043001.

Sonia Jain and Radford M Neal. Splitting and merging components of a nonconjugate Dirichlet process mixture model. *Bayesian Analysis*, 2(3):445–472, 2005. ISSN 19360975. doi: 10.1214/07-BA219.

Sushrut Jangi and J. Thomas Lamont. Asymptomatic colonization by Clostridium Difficile in infants: Implications for disease in later life. *Journal of Pediatric Gastroenterology and Nutrition*, 51(1):2–7, 2010. ISSN 02772116. doi: 10.1097/MPG.0b013e3181d29767.

Valen E. Johnson and David Rossell. On the use of non-local prior densities in Bayesian hypothesis tests. *Journal of the Royal Statistical Society. Series B: Statistical Methodology*, 72(2):143–170, 2010. ISSN 13697412. doi: 10.1111/j.1467-9868.2009.00730.x.

Michael I. Jordan and David M. Blei. Variational inference for Dirichlet process mixtures. *Bayesian Analysis*, 1(1):121–143, 2006. ISSN 1936-0975. doi: 10.1214/06-BA104.

Sinae Kim, David B. Dahl, and Marina Vannucci. Spiked Dirichlet process prior for Bayesian multiple hypothesis testing in random effects models. *Bayesian Analysis*, 4(4):707–732, 2009. ISSN 19360975. doi: 10.1214/09-BA426. URL http://www.pubmedcentral.nih.gov/articlerender.fcgi?artid=3741668{&}tool=pmcentrez{&}rendertype=abstract.

Athanasios Kottas and Gilbert W. Fellingham. Bayesian semiparametric modeling and inference with mixtures of symmetric distributions. *Statistics and Computing*, 22

(1):93–106, 2012. ISSN 09603174. doi: 10.1007/s11222-010-9208-x. URL http://link.springer.com/10.1007/s11222-010-9208-x.

Ruiting Lan and Peter R. Reeves. Escherichia coli in disguise: Molecular origins of Shigella. *Microbes and Infection*, 4(11):1125–1132, 2002. ISSN 12864579. doi: 10.1016/S1286-4579(02)01637-4.

Antonio Lijoi, Ramsés H. Mena, and Igor Prünster. Controlling the reinforcement in Bayesian non-parametric mixture models. *Journal of the Royal Statistical Society. Series B: Statistical Methodology*, 69(4):715–740, 2007. ISSN 13697412. doi: 10.1111/j.1467-9868.2007.00609.x. URL http://doi.wiley.com/10.1111/j.1467-9868.2007.00609.x.

Ryan Martin and Surya T. Tokdar. A nonparametric empirical Bayes framework for large-scale multiple testing. *Biostatistics*, 13(3):427–439, 2012. ISSN 14654644. doi: 10.1093/biostatistics/kxr039.

Patrick Muller, Giovanni Parmigiani, and Kenneth Rice. FDR and Bayesian multiple comparisons rules. In José M Bernardo, M J Bayarri, James O Berger, A P Dawid, D Heckerman, Mike West, and Adrian F M Smith, editors, *Bayesian Statistics 8*, number 1995, pages 349–370. Oxford University Press, 2006. URL http://biostats.bepress.com/jhubiostat/paper115/.

Omkar Muralidharan. An empirical Bayes mixture method for effect size and false discovery rate estimation. *Annals of Applied Statistics*, 6(1):422–438, 2012. ISSN 19326157. doi: 10.1214/09-AOAS276. URL http://projecteuclid.org/euclid.aoas/1273584461.

Radford M Neal. Markov Chain sampling methods for Dirichlet process mixture models. *Journal of Computational and Graphical Statistics*, 9(2):249–265, 2000.

Michael A. Newton, Amine Noueiry, Deepayan Sarkar, and Paul Ahlquist. Detecting differential gene expression with a semiparametric hierarchical mixture method. *Biostatistics*, 5(2):155–176, 2004. ISSN 14654644. doi: 10.1093/biostatistics/5.2.155. URL http://www.ncbi.nlm.nih.gov/pubmed/15054023.

Jim Pitman. Exchangeable and partially exchangeable random partitions. *Probability Theory and Related Fields*, 102:145–158, 1995.

Jim Pitman. *Combinatorial Stochastic Processes*. Springer-Verlag, 2002. ISBN 9783540309901. URL http://link.springer.com/content/pdf/10.1007/b11601500.pdf.

Mihai Pop, Joseph N. Paulson, Hector Corrada Bravo, et al. Diarrhea in young children from low-income countries leads to large-scale alterations in intestinal microbiota composition. *Genome Biol*, 15(6):R76, 2014. ISSN -5441. doi: 10.1186/gb-2014-15-6-r76.

Gareth O. Roberts and Jeffrey S. Rosenthal. Examples of adaptive MCMC. *Journal of Computational and Graphical Statistics*, 18(2):349–367, 2009. ISSN 10618600. doi: 10.1198/jcgs.2009.06134.

David Rossell and Donatello Telesca. Nonlocal priors for high-dimensional estimation. *Journal of the American Statistical Association*, 112(517):254–265, 2017. ISSN 1537274X. doi: 10.1080/01621459.2015.1130634. URL `https://doi.org/10.1080/01621459.2015.1130634`.

Dinesh Singh, Phillip G. Febbo, Kenneth Ross, Donald G. Jackson, Judith Manola, Christine Ladd, Pablo Tamayo, Andrew A. Renshaw, Anthony V. D'Amico, Jerome P. Richie, Eric S. Lander, Massimo Loda, Philip W. Kantoff, Todd R. Golub, and William R. Sellers. Gene expression correlates of clinical prostate cancer behavior. *Cancer Cell*, 1(2):203–209, 2002. ISSN 15356108. doi: 10.1016/S1535-6108(02)00030-2.

Alexander Swidsinski, Vera Loening-Baucke, Hans Verstraelen, Sylwia Osowska, and Yvonne Doerffel. Biostructure of fecal microbiota in healthy subjects and patients with chronic idiopathic diarrhea. *Gastroenterology*, 135(2)(2):568–79, 2008. ISSN 00165085. doi: 10.1053/j.gastro.2008.04.017.

Daniela M. Witten. Classification and clustering of sequencing data using a Poisson model. *Annals of Applied Statistics*, 5(4):2493–2518, 2011. ISSN 19326157. doi: 10.1214/11-AOAS493. URL `http://projecteuclid.org/euclid.aoas/1324399604`.

Natalya Yutin and Michael Y Galperin. A genomic update on clostridial phylogeny: Gram-negative spore formers and other misplaced clostridia. *Environmental microbiology*, 15(10):2631–41, 2013. ISSN 1462-2920. doi: 10.1111/1462-2920.12173. URL `http://www.ncbi.nlm.nih.gov/pubmed/23834245{%}0Ahttp://www.pubmedcentral.nih.gov/articlerender.fcgi?artid=PMC4056668`.

Supporting Information

The code is openly available online at `https://github.com/mguindanigroup/twogroup2PPD`.

Table 1: Simulation study: sensitivity results across different settings for σ_0 and σ_1 for the five simulation scenarios considered in Section 4.1 ($\rho = 0.05$). The values in the table represent the average MCC and F_1 scores, the average precision (PRE), specificity (SPEC), accuracy (ACC) and the area under the curve (AUC) of the corresponding receiver operating characteristic curve, over 30 replicates with corresponding standard deviations between brackets.

	$\sigma_0 = 0.75$						$\sigma_0 = 0.9$	
	$\sigma_1 = 0$		$\sigma_1 = 0.1$		$\sigma_1 = 0.25$		$\sigma_1 = 0.25$	
Scenario 1								
MCC	0.5777	(0.0903)	0.5833	(0.0940)	0.6020	(0.0835)	0.5893	(0.0876)
F1	0.5197	(0.1125)	0.5269	(0.1169)	0.5520	(0.1051)	0.5342	(0.1095)
AUC	0.9095	(0.0245)	0.9143	(0.0224)	0.9201	(0.0253)	0.9200	(0.0207)
PRE	0.9775	(0.0357)	0.9773	(0.0333)	0.9713	(0.0346)	0.9776	(0.0328)
SPEC	0.9995	(0.0007)	0.9995	(0.0007)	0.9994	(0.0008)	0.9995	(0.0007)
ACC	0.9676	(0.0049)	0.9680	(0.0052)	0.9690	(0.0048)	0.9683	(0.0049)
Scenario 2								
MCC	0.6249	(0.0673)	0.6242	(0.0695)	0.6212	(0.0681)	0.6135	(0.0644)
F1	0.5809	(0.0831)	0.5796	(0.0855)	0.5771	(0.0835)	0.5665	(0.0808)
AUC	0.9526	(0.0218)	0.9563	(0.0185)	0.9581	(0.0170)	0.9523	(0.0183)
PRE	0.9710	(0.0338)	0.9725	(0.0373)	0.9680	(0.0396)	0.9712	(0.0384)
SPEC	0.9993	(0.0008)	0.9994	(0.0009)	0.9993	(0.0009)	0.9993	(0.0009)
ACC	0.9703	(0.0043)	0.9703	(0.0044)	0.9701	(0.0043)	0.9696	(0.0040)
Scenario 3								
MCC	0.5081	(0.0842)	0.5080	(0.0847)	0.5340	(0.0797)	0.5224	(0.0808)
F1	0.4320	(0.1053)	0.4320	(0.1056)	0.4659	(0.1001)	0.4489	(0.1018)
AUC	0.9335	(0.0235)	0.9401	(0.0238)	0.9477	(0.0180)	0.9452	(0.0209)
PRE	0.9721	(0.0438)	0.9714	(0.0425)	0.9682	(0.0402)	0.9772	(0.0360)
SPEC	0.9995	(0.0007)	0.9995	(0.0007)	0.9994	(0.0007)	0.9996	(0.0006)
ACC	0.9624	(0.0044)	0.9624	(0.0045)	0.9638	(0.0045)	0.9631	(0.0043)
Scenario 4								
MCC	0.7513	(0.0462)	0.7554	(0.0462)	0.7625	(0.0461)	0.7572	(0.0478)
F1	0.7354	(0.0538)	0.7413	(0.0528)	0.7535	(0.0518)	0.7449	(0.0542)
AUC	0.9552	(0.0162)	0.9627	(0.0119)	0.9685	(0.0107)	0.9661	(0.0087)
PRE	0.9787	(0.0264)	0.9736	(0.0284)	0.9532	(0.0312)	0.9657	(0.0289)
SPEC	0.9993	(0.0009)	0.9991	(0.0010)	0.9984	(0.0013)	0.9988	(0.0010)
ACC	0.9789	(0.0034)	0.9792	(0.0035)	0.9797	(0.0035)	0.9794	(0.0036)
Scenario 5								
MCC	0.8920	(0.0229)	0.8832	(0.0249)	0.8529	(0.0232)	0.8694	(0.0241)
F1	0.8951	(0.0219)	0.8860	(0.0241)	0.8534	(0.0235)	0.8710	(0.0238)
AUC	0.9985	(0.0010)	0.9985	(0.0010)	0.9985	(0.0011)	0.9985	(0.0011)
PRE	0.8346	(0.0300)	0.8170	(0.0334)	0.7560	(0.0330)	0.7856	(0.0326)
SPEC	0.9898	(0.0021)	0.9885	(0.0025)	0.9832	(0.0029)	0.9859	(0.0026)
ACC	0.9886	(0.0020)	0.9875	(0.0028)	0.9831	(0.0030)	0.9855	(0.0029)

Table 2: Simulation study: performance metrics for five other multiple comparison methods in the five simulation scenarios considered in Section 4.1 ($\rho = 0.05$). The values in the table represent the average MCC and F_1 scores, the average precision (PRE), specificity (SPEC), accuracy (ACC) and the area under the curve (AUC) of the corresponding receiver operating characteristic curve, over 30 replicates with corresponding standard deviations between brackets.

	DPmix		*local fdr*		Benjamini and Hochberg [1995]		Muralidharan [2012]		Martin and Tokdar [2012]	
Scenario 1										
MCC	0.2329	(0.0209)	0.5708	(0.0721)	0.6629	(0.0648)	0.5379	(0.0804)	0.5835	(0.0757)
F1	0.1980	(0.0145)	0.5067	(0.0932)	0.6427	(0.0736)	0.4643	(0.1023)	0.5251	(0.0962)
AUC	0.9053	(0.0301)	0.8869	(0.0365)	0.9237	(0.0205)	0.9242	(0.0230)	0.9230	(0.0216)
PRE	0.1113	(0.0092)	0.9897	(0.0216)	0.9141	(0.0603)	0.9915	(0.0227)	0.9825	(0.0284)
SPEC	0.6150	(0.0432)	0.9998	(0.0004)	0.9974	(0.0019)	0.9999	(0.0004)	0.9996	(0.0006)
ACC	0.6297	(0.0396)	0.9671	(0.0042)	0.9726	(0.0044)	0.9653	(0.0043)	0.9679	(0.0044)
Scenario 2										
MCC	0.2506	(0.0180)	0.6088	(0.0773)	0.6674	(0.0638)	0.5805	(0.0667)	0.6435	(0.0686)
F1	0.2037	(0.0138)	0.5578	(0.0991)	0.6486	(0.0721)	0.5194	(0.0857)	0.6048	(0.0846)
AUC	0.9524	(0.0218)	0.9231	(0.0428)	0.9544	(0.0169)	0.9668	(0.0174)	0.9762	(0.0087)
PRE	0.1140	(0.0087)	0.9796	(0.0304)	0.9129	(0.0556)	0.9895	(0.0216)	0.9698	(0.0332)
SPEC	0.6033	(0.0364)	0.9995	(0.0008)	0.9974	(0.0018)	0.9998	(0.0004)	0.9993	(0.0008)
ACC	0.6213	(0.0339)	0.9694	(0.0048)	0.9729	(0.0042)	0.9676	(0.0004)	0.9715	(0.0044)
Scenario 3										
MCC	0.2337	(0.0195)	0.5397	(0.0854)	0.6544	(0.0578)	0.4840	(0.0883)	0.5591	(0.0740)
F1	0.1948	(0.0129)	0.4708	(0.1087)	0.6342	(0.0670)	0.3973	(0.1080)	0.4970	(0.0948)
AUC	0.9400	(0.0206)	0.9069	(0.0359)	0.9500	(0.0191)	0.9481	(0.0197)	0.9481	(0.0182)
PRE	0.1085	(0.0079)	0.9759	(0.0424)	0.9089	(0.0561)	0.9901	(0.0328)	0.9707	(0.0437)
SPEC	0.5679	(0.0349)	0.9995	(0.0008)	0.9972	(0.0020)	0.9999	(0.0005)	0.9994	(0.0010)
ACC	0.5880	(0.033)	0.9641	(0.0050)	0.9710	(0.0040)	0.9611	(0.0043)	0.9652	(0.0044)
Scenario 4										
MCC	0.2671	(0.0194)	0.7080	(0.0474)	0.7849	(0.0443)	0.6840	(0.0486)	0.6831	(0.0470)
F1	0.2161	(0.0156)	0.6801	(0.0586)	0.7853	(0.0448)	0.6492	(0.0602)	0.6485	(0.0595)
AUC	0.9612	(0.0156)	0.9406	(0.0246)	0.9709	(0.0085)	0.9627	(0.0159)	0.9658	(0.0139)
PRE	0.1217	(0.0099)	0.9919	(0.0172)	0.9136	(0.0502)	0.9972	(0.0106)	0.9953	(0.0123)
SPEC	0.6288	(0.0345)	0.9998	(0.0005)	0.9965	(0.0023)	0.9999	(0.0003)	0.9999	(0.0004)
ACC	0.6459	(0.0325)	0.9758	(0.0033)	0.9812	(0.0036)	0.9741	(0.0034)	0.9741	(0.0032)
Scenario 5										
MCC	0.2671	(0.0194)	0.8632	(0.0492)	0.7861	(0.0360)	0.8506	(0.0486)	0.8879	(0.0332)
F1	0.5303	(0.0420)	0.8611	(0.0529)	0.7792	(0.0395)	0.8475	(0.0414)	0.8888	(0.0338)
AUC	0.9980	(0.0012)	0.9971	(0.0041)	0.9986	(0.0010)	0.9985	(0.0012)	0.9985	(0.0011)
PRE	0.3622	(0.0163)	0.9811	(0.0286)	0.6433	(0.0531)	0.9866	(0.0229)	0.9745	(0.0323)
SPEC	0.9058	(0.0155)	0.9992	(0.0013)	0.9705	(0.0067)	0.9994	(0.0009)	0.9988	(0.0015)
ACC	0.9104	(0.0385)	0.9878	(0.0041)	0.9716	(0.0064)	0.9867	(0.0032)	0.9899	(0.0028)

Web Appendix A: Posterior inference

In this Section, we detail the MCMC algorithm for posterior inference for model (6) and model (8)–(9), with particular regards to inference on the auxiliary variable indicators γ_i's and the two-group components' weight ρ.

Before deriving the full conditional distributions, we first need to outline a few properties of the clustering implied by the EPPF (7). More specifically, an underlying assumption of the two-group model is that if two observations assume the same value, they should not be assigned to different groups. For the 2PPD processes, the following result holds

LEMMA 1. *If $Z_1, \ldots, Z_n$ are a random sample from an exchangeable sequence $\boldsymbol{Z}$ governed by a random probability measure as defined in (6), with P_j^*, $j = 0, 1$, being non-atomic base measures with common support, then*

$$\mathbb{P}[Z_i = Z_j \mid \gamma_i \neq \gamma_j] = 0$$

for $i \neq j$.

The result follows directly from the characterization of the 2PPD process as an infinite mixture and the fact that P_j^* is non-atomic. A notable consequence of this result is that Z_i's belonging to the same cluster are generated by the same PD process. In the case of the 2PPD mixture models (9), Lemma 1 applies to the atoms generated by the nonparametric priors. Given the same set of hypotheses, we have that

$$\mathbb{P}[\boldsymbol{\vartheta}_i = \boldsymbol{\vartheta}_j \mid \gamma_i \neq \gamma_j] = 0.$$

As we outline below, this result is crucial for a proper characterization of the full conditionals of each model.

- **MCMC for model (6):** At any iteration of the MCMC algorithm, the vector of observations $\boldsymbol{Z} = (Z_1, \ldots, Z_n)$ is partitioned into K separate clusters, $K \geq 1$. Let $Z_1^*, \ldots, Z_K^*$ denote the $K \leq n$ unique values in $\boldsymbol{Z}$. We denote the corresponding partition sets by $C_{k,n} = \{i : Z_i = Z_k^*\}$, $k = 1, \ldots, K$, and by $n_k = |C_{k,n}|$, the cardinality of each set. By virtue of Lemma 1, two observations assigned to the same cluster are also assigned to the same random probability measure. Therefore, let γ_k^* be an auxiliary random variable such that $\gamma_k^* = 0$ if the partition set $C_{k,n}$ contains draws from $\tilde{p}_0$ and $\gamma_k^* = 1$ otherwise. Then, for any $i \in C_{k,n}$, one has $\gamma_i = \gamma_k^*$, and, conditional on the partition sets $C_{k,n}$, $k = 1, \ldots, K$, the K-tuple $\boldsymbol{\gamma}^* = (\gamma_1^*, \ldots, \gamma_K^*) \in \{0, 1\}^K$ describes the solution of the multiple testing problem, analogously to the vector $\boldsymbol{\gamma} = (\gamma_1, \ldots, \gamma_n) \in \{0, 1\}^n$. Then, posterior samples for $\boldsymbol{\gamma}$ can be immediately derived from the posterior samples of the vector $\boldsymbol{\gamma}^*$ and the configuration of the partition sets $C_{k,n}$, $k = 1, \ldots, K$, which can be obtained by means of a Gibbs sampling scheme.

More specifically, let us consider the joint probability distribution of the vector $\boldsymbol{\gamma} = (\gamma_1, \ldots, \gamma_n)$, and the partition $\boldsymbol{C}_n = \{C_{1,n}, \ldots, C_{K,n}\}$,

$$\mathscr{L}(\boldsymbol{\gamma}, C_{1,n}, \ldots, C_{K,n}) = \mathscr{L}(\boldsymbol{\gamma})\, \mathscr{L}(C_{1,n}, \ldots, C_{K,n} \mid \boldsymbol{\gamma}).$$

The joint distribution of $\boldsymbol{\gamma}$ can be obtained as

$$\mathscr{L}(\boldsymbol{\gamma}) = \frac{(a)_{|\boldsymbol{\gamma}|}(b)_{n-|\boldsymbol{\gamma}|}}{(a+b)_n}, \tag{9}$$

where $|\boldsymbol{\gamma}| = \sum \gamma_i$. Here, $|\boldsymbol{\gamma}|$ indicates the number of observation currently assigned to the non-null process. By Lemma 1 and Proposition 1, the conditional distribution of $C_{1,n}, \ldots, C_{K,n}$ given $\boldsymbol{\gamma}$ can be written as

$$\begin{aligned} \mathscr{L}(C_{1,n}, \ldots, C_{K,n} \mid \boldsymbol{\gamma}) &= \mathscr{L}(C_{1,n}, \ldots, C_{K,n} \mid \boldsymbol{\gamma}^*) \\ &= \Pi_{K_0,0}^{(n-|\boldsymbol{\gamma}|)}(n_1(1-\gamma_1^*), \ldots, n_K(1-\gamma_K^*)) \\ &\times\ \Pi_{K_1,1}^{(|\boldsymbol{\gamma}|)}(n_1\gamma_1^*, \ldots, n_K\gamma_K^*) \prod_{k=1}^{K} \prod_{i \in C_{k,n}} \mathbb{1}_{\{\gamma_k^*\}}(K_i), \end{aligned} \tag{10}$$

where $K_1 = \sum_{k=1}^{K} \gamma_k^*$ and $K_0 = K - K_1$ indicate the number of clusters belonging to $\tilde{p}_1$ and to $\tilde{p}_0$, respectively. Expression (9) and (10) emphasize that it is sufficient to consider only the cluster-based vector of indicators $\boldsymbol{\gamma}^*$ in order to determine the joint probability distribution of the $\boldsymbol{\gamma}$ and the partition $\boldsymbol{C}_n$. Therefore, in order to obtain the full conditional distribution of the γ_i's, we may focus only on the γ_k^*'s and the vector of $K \leq n$ observations in $\boldsymbol{Z}^*$. Let $\boldsymbol{\gamma}_{-k}^*$ denote the $\boldsymbol{\gamma}^*$ vector with the kth entry removed. Similarly, we define $\boldsymbol{\gamma_{-i}}$ as the vector where the ith entry is deleted. This implies that $\boldsymbol{\gamma}_{-k}^* \in \{0,1\}^{K-1}$ and that $\boldsymbol{\gamma}_{-i} \in \{0,1\}^{n-1}$. Also let $n_{-k,1} = \sum_{l \neq k}^{K} n_l \gamma_l^*$ denote the number of observations not included in $C_{k,n}$ which at the same time come from the non-null process. Furthermore, for any $k = 1, \ldots, K$, let $K_{-k,1} = |\boldsymbol{\gamma}_{-i}^*| = \sum_{l \neq k}^{K} \gamma_l^*$ indicate the number of clusters assigned to the non-null distribution $\tilde{p}_1$ after removing cluster $C_{k,n}$.

We can now write the full conditional of the γ_k^*'s. For notational simplicity, let $\gamma_k^* = \xi$, where $\xi \in \{0,1\}$. Then, the full conditional $\mathscr{L}_k(\xi \mid \boldsymbol{\gamma}_{-k}^*, \boldsymbol{Z}^*, \boldsymbol{C}_n) \propto p_{k,\xi}$ where

$$\begin{aligned} p_{k,\xi} &= (a)_{n_{-k,1}+n_k\xi}(b)_{n-n_{-k,1}-n_k\xi}\, P_\xi^*(\mathrm{d}Z_k^*) \prod_{j \neq k} P_{\gamma_j^*}^*(\mathrm{d}Z_j^*) \prod_{l \in C_{k,n}} \mathbb{1}_{\{\gamma_k^*\}}(\gamma_l) \\ &\times\ \Pi_{K-K_{-k,1}-\xi,0}^{(n-n_{-k,1}-n_k\xi)}(n_1(1-\gamma_1^*), \ldots, n_k(1-\xi), \ldots, n_K(1-\gamma_K^*)) \\ &\times\ \Pi_{K_{-k,1}+\xi,1}^{(n_{-k,1}+n_k\xi)}(n_1\gamma_1^*, \ldots, n_k\xi, \ldots, n_K\gamma_K^*). \end{aligned}$$

In particular, the probability $P(\gamma_k^* = 1 \mid \boldsymbol{\gamma}_{-k}^*, \boldsymbol{Z}^*, \boldsymbol{C}_n)$ determines the probability that for any $i \in C_{k,n}$, the observations $Z_i = Z_k^*$ are assigned to the non-null

distribution, and can be obtained as

$$\mathscr{L}_k(\xi = 1 \mid \boldsymbol{\gamma}^*_{-k}, \boldsymbol{Z}^*, \boldsymbol{C}_n) = \frac{1}{1 + (p_{k,0}/p_{k,1})},$$

where the ratio

$$\begin{aligned}\frac{p_{k,0}}{p_{k,1}} = \frac{P^*_0(\mathrm{d}Z^*_k)}{P^*_1(\mathrm{d}Z^*_k)} \, \frac{\Gamma(a + n_{-k,1})}{\Gamma(a + n_{-k,1} + n_k)} \, \frac{\Gamma(b + n - n_{-k,1})}{\Gamma(b + n - n_{-k,1} - n_k)} \\ \times \, \frac{\Pi^{(n-n_{-k,1})}_{K-K_{-k,1},0}(n_1(1-\gamma^*_1), \ldots, n_k, \ldots, n_K(1-\gamma^*_K))}{\Pi^{(n-n_{-k,1}-n_k)}_{K-K_{-k,1}-1,0}(n_1(1-\gamma^*_1), \ldots, n_K(1-\gamma^*_K))} \\ \times \, \frac{\Pi^{(n_{-k,1})}_{K_{-k,1},1}(n_1\gamma^*_1, \ldots, n_K\gamma^*_K)}{\Pi^{(n_{-k,1}+n_k)}_{K_{-k,1}+1,1}(n_1\gamma^*_1, \ldots, n_k, \ldots, n_K\gamma^*_K)}.\end{aligned}$$

The previous expression is valid for all normalized random measures with independent increments. If $\tilde{p}_j$ is a 2PPD$(\sigma_j, \theta_j, P^*_j)$, $j = 0, 1$ process, then the above ratio further simplifies as:

$$\begin{aligned}\frac{p_{k,0}}{p_{k,1}} = \frac{P^*_0(\mathrm{d}Z^*_k)}{P^*_1(\mathrm{d}Z^*_k)} \, \frac{(b + n - n_{-k,1} - n_k)_{n_k}}{(a + n_{-k,1})_{n_k}} \, \frac{(1-\sigma_0)_{n_k-1}}{(1-\sigma_1)_{n_k-1}} \\ \times \, \frac{\theta_0 + (K - K_{-k,1} - 1)\,\sigma_0}{\theta_1 + K_{-k,1}\,\sigma_1} \, \frac{(\theta_1 + n_{-k,1})_{n_k}}{(\theta_0 + n - n_{-k,1} - n_k)_{n_k}}. \quad (11)\end{aligned}$$

It is worth noting that if the two base measures coincide, i.e., $P^*_0 = P^*_1$, then the full conditional does not depend on Z^*_k; therefore, the probability that Z^*_k is a draw from the non-null depends only on the clustering behavior of the 2PPD process implied by the parameters characterizing $\tilde{p}_0$ and $\tilde{p}_1$.

To summarize, in order to implement a Gibbs sampler for sampling the auxiliary indicators in (6), at each iteration $t = 1, \ldots, T$, we draw each γ^*_k, from the full conditional $\mathscr{L}_k(\xi = 1 \mid \boldsymbol{\gamma}^*_{-k}, \boldsymbol{Z}^*, \boldsymbol{C}_n)$. The vectors $\boldsymbol{\gamma}^*_t$, $t = 1, \ldots, T$, can then be mapped to the vector $\boldsymbol{\gamma}$ using the partition sets $\boldsymbol{C}_n$.

- **MCMC for model (8)–(9):** The full conditionals for the vectors γ^*_k are derived in a similar way as above. More specifically, for $\gamma^*_k = \xi$, let $\vartheta^*_{k,\xi} \sim P^*_\xi$, indicate an atom of $\tilde{p}_\xi$, $\xi \in \{0, 1\}$, $k = 1, \ldots K$. Then,

$$\begin{aligned}&\mathscr{L}[\xi \mid \boldsymbol{\gamma}^*_{-k}, C_{1,n}, \ldots, C_{K,n}, \boldsymbol{Z}] \\ &\propto \left\{ \int \prod_{l \in C_{k,n}} k_\xi\left(\boldsymbol{Z}_l | \vartheta^*_{k,\xi}\right) \, P^*_\xi(\mathrm{d}\vartheta^*_{k,\xi}) \right\} \Gamma(a + n_{-k,1} + n_k\xi)\Gamma(b + n - n_{-k,1} - n_k\xi)\end{aligned}$$

$$\times\ \Pi^{(n-n_{-k,1}-n_k\xi)}_{K-K_{-k,1}-\xi,0}(n_1(1-\gamma_1^*),\ldots,n_k(1-\xi),\ldots,n_K(1-\gamma_K^*))$$
$$\times\ \Pi^{(n_{-k,1}+n_k\xi)}_{K_{-k,1}+\xi,1}(n_1\gamma_1^*,\ldots,n_k\xi,\ldots,n_K\gamma_K^*)\prod_{l\in C_{k,n}}\mathbb{1}_{\{\xi\}}(\gamma_l),$$

If we denote with $f_{k,\xi}$ the marginal likelihoods

$$\pi\left(\boldsymbol{Z}_{l\in C_{k,n}}\right)=\left\{\int\prod_{l\in C_{k,n}}k_\xi\left(X_l|\boldsymbol{\vartheta}^*_{k,\xi}\right)\ P^*_\xi(\mathrm{d}\boldsymbol{\vartheta}^*_{k,\xi})\right\}$$

we can recover an expression similar to (11):

$$\frac{p_{k,0}}{p_{k,1}}=\frac{f_{k,0}}{f_{k,1}}\,\frac{(b+n-n_{-k,1}-n_k)_{n_k}}{(a+n_{-k,1})_{n_k}}\,\frac{(1-\sigma_0)_{n_k-1}}{(1-\sigma_1)_{n_k-1}}$$
$$\times\ \frac{\theta_0+(K-K_{-k,1}-1)\sigma_0}{\theta_1+K_{-k,1}\,\sigma_1}\,\frac{(\theta_1+n_{-k,1})_{n_k}}{(\theta_0+n-n_{-k,1}-n_k)_{n_k}}. \quad (12)$$

Since ρ is conditionally independent from the observations Z_i's given the γ_i's and the parameter $\boldsymbol{\vartheta}_i$, we can obtain the full conditional distribution of ρ as

$$\mathcal{L}[\mathrm{d}\rho\mid Z_1,\ldots,Z_n,\boldsymbol{\vartheta}_1,\ldots,\boldsymbol{\vartheta}_n,\gamma_1,\ldots,\gamma_n]$$
$$=\frac{\Gamma(a+b+n)}{\Gamma(a+n^*)\Gamma(b+n-n^*)}\rho^{a+n^*-1}(1-\rho)^{b+n-n^*-1}\,\mathbb{1}_{(0,1)}(\rho),$$

that is, as a sample from a Beta$(a+n^*,b+n-n^*)$, with $n^*=\sum_{j=1}^K n_j\gamma_j^*$. The sampling algorithm is then completed by drawing samples of the $\boldsymbol{\vartheta}_i^*$'s from the respective full conditionals.

The full conditional of $\boldsymbol{\vartheta}_i$ is obtained as

$$\mathscr{L}[\mathrm{d}\boldsymbol{\vartheta}_{i,\gamma_i}\mid\boldsymbol{\vartheta}_{-i},\boldsymbol{\gamma}^*,\boldsymbol{C}_n,\boldsymbol{Z}]\propto q_0^{(i)}\,\frac{k_{\gamma_i}(Z_i\mid\boldsymbol{\vartheta}_{i,\gamma_i})\,P^*_{\gamma_i}(\mathrm{d}\boldsymbol{\vartheta}_{i,\gamma_i})}{\int_{\mathbb{R}\times\mathbb{R}^+}k_{\gamma_i}(Z_i\mid\boldsymbol{\vartheta_{i,\gamma_i}})\,P^*_{\gamma_i}(\mathrm{d}\boldsymbol{\vartheta_{i,\gamma_i}})}$$
$$+\sum_{j=1}^{\kappa^{(-i)}_{\gamma_i}}q_j^{(i)}\,\delta_{\boldsymbol{\vartheta}^*_{j,\gamma_i}}(\mathrm{d}\boldsymbol{\vartheta}_{i,\gamma_i})$$

where $\boldsymbol{\vartheta}_{-i}=\{(\mu_j,\tau_j^2)_{\gamma_j}:\ j\neq i\}$ and $\kappa^{(-i)}_{\gamma_i}$ is the number of unique values in $\boldsymbol{\vartheta}_{-i}$ that share the same generating random probability measure $\tilde{p}_{\gamma_i}$ with $\boldsymbol{\vartheta}_{i,\gamma_i}$. Correspondingly, the respective frequencies are denoted as $\boldsymbol{n}^{(-i)}_{\gamma_i}=\left(n^{(-i)}_{1,\gamma_i},\ldots,n^{(-i)}_{\kappa_{\gamma_i},\gamma_i}\right)$ with weights $q_0^{(i)}$ and $q_j^{(i)}$ as follows

$$q_0^{(i)}\propto\Pi^{(|n^{(-i)}_{\gamma_i}|+1)}_{\kappa^{(-i)}_{\gamma_i}+1,\gamma_i}(n^{(-i)}_{1,\gamma_i},\ldots,n^{(-i)}_{\kappa_{\gamma_i},\gamma_i},1)\,k_{\gamma_i}(Z_i\mid\boldsymbol{\vartheta}_i)$$

$$q_j^{(i)} \propto \Pi^{(|n_{\gamma_i}^{(-i)}|+1)}_{\kappa_{\gamma_i}^{(-i)},\gamma_i}(n_{1,\gamma_i}^{(-i)},\ldots,n_{j,\gamma_i}^{(-i)}+1,\ldots,n_{\kappa_{\gamma_i}^{(-i)},\gamma_i}^{(-i)})$$

Specializing the previous formula to the 2PPD process, we obtain:

$$q_0^{(i)} \propto \left(\theta_{\gamma_i}+\kappa_{\gamma_i}^{(-i)}\sigma_{\gamma_i}\right) \int k_{\gamma_i}\left(Z_i \mid \boldsymbol{\vartheta}_i\right) P^*_{\gamma_i}\left(d\boldsymbol{\vartheta}_i\right),$$
$$q_j^{(i)} \propto \left(n_{j,\gamma_i}^{(-i)}-\sigma_{\gamma_i}\right) k_{\gamma_i}\left(Z_i \mid \vartheta^*_{j,\gamma_i}\right).$$

where $\int k_{\gamma_i}\left(Z_i \mid \boldsymbol{\vartheta}_i\right) P^*\left(d\boldsymbol{\vartheta_i}\right)$ is the marginal likelihood based only on the observation Z_i

Finally, the full conditional for m_1 is sampled with a simple adaptive Metropolis Hasting step [Roberts and Rosenthal, 2009]. Here, we can take advantage of the conjugacy properties of the model and employ a marginal Gibbs sampler as discussed in Ishwaran and James [2001]. Alternatively, for non-conjugate models, a Metropolis-Hastings algorithm would be equivalently straightforward to implement, and mimic widely used algorithms for Dirichlet Process mixture models [Neal, 2000].

- **Implementation of the Split-Merge move for model (8)-(9)**: In the cases of Dirichlet and Pitman-Yor process mixture models, posterior sampling is often performed via Gibbs sampler. Unfortunately, especially in marginal models, the Gibbs sampler explores the state space by means of conditional updates cycling through all observations and can get stuck in local modes. Thus, it can mix poorly across modes that have high probability [Dahl, 2003]. To address the deficiencies of the Gibbs sampler, Jain and Neal [2004, 2005] propose a split-merge (SM) algorithm which greatly improves the mixing. To obtain the best performance, they recommend to cycle between the usual Gibbs sampler and their SM proposal. Nevertheless, their sampler is known to be computationally demanding. To obviate this problem, Dahl proposes an enhanced versions of the first split-merge sampler, called SAMS, that can be used in conjugate cases [Dahl, 2003] and in non-conjugate cases [Dahl, 2005] for Dirichlet Process mixture models.

  In the following, we adapt the conjugate version of Dahl's SM sampler to be employed in Pitman-Yor mixture models. In particular, according to Lemma 1, given the process allocation variables $\boldsymbol{\gamma}$, the two processes are independent. This allows us to perform two separate Split and Merge steps, one per process. In the following, we present the sampler for the generic process γ', $\gamma' = 0, 1$. Let us denote the partition observed among the observations with $\eta = \{S_1, S_2, \ldots, S_{K^*}\}$, where S_l denotes the subset of indexes assigned to the l-th cluster and K^* denotes the number of subsets in the partition.

  Steps

  1. Among the observations assigned to the same process γ', uniformly select a pair of distinct indices i and j.

2. If i and j belong to the same component in η , propose $\eta^{\star}$ by attempting a split move:

   S1 For convenience, denote the common component containing indexes i and j as S. Remove the indexes i and j from S and form singleton sets $S_i = \{i\}$ and $S_j = \{j\}$.

   S2 Letting k be successive values in a **uniformly-selected permutation** of the indexes in S, add k to S_i with probability

$$Pr\left(k \in S_i | S_i, S_j, y\right) = \frac{\left(n_{i,\gamma} - \sigma_{\gamma}\right) \int F\left(y_k; \vartheta\right) dH_{S_i}(\vartheta)}{\left(n_{i,\gamma} - \sigma_{\gamma}\right) \int F\left(y_k; \vartheta\right) dH_{S_i}(\vartheta) + \left(n_{j,\gamma} - \sigma_{\gamma}\right) \int F\left(y_k; \vartheta\right) dH_{S_j}(\vartheta)},$$

   where H_S is the posterior distribution of a component location ϑ based on the prior $P^*_{\gamma'}$ and the data corresponding to the indices in S . Otherwise, add k to S_j . Note that, at each iteration above, either S_i or S_j gains an index resulting in $n_{i,\gamma'}$ or $n_{j,\gamma'}$ increasing by 1 . Further, H_{S_i} and H_{S_j} evolve to account for each additional index. We remark how our model employs non-conjugate base measures for the Null process. However, it is straightforward to perform precise numerical integration over the parameters' space. Working with marginal distributions $m_{\gamma'}\left(S_l\right)$ of all the observations in the l-th cluster, we can rewrite

$$\begin{aligned} \int F\left(y_k; \vartheta\right) dH_{S_i}(\vartheta) &= \int F\left(y_k; \vartheta\right) \frac{F\left(S_i; \vartheta\right) P^*_{\gamma'}(\vartheta) d\vartheta}{m_{\gamma'}\left(S_i\right)} \\ &= \frac{m_{\gamma'}\left(y_k, S_i\right)}{m_{\gamma'}\left(S_i\right)} \end{aligned}$$

   and consequently

$$Pr\left(k \in S_i | S_i, S_j, y\right) = \frac{\left(n_{i,\gamma'} - \sigma_{\gamma'}\right) \frac{m_{\gamma'}(y_k, S_i)}{m_{\gamma'}(S_i)}}{\left(n_{i,\gamma'} - \sigma_{\gamma'}\right) \frac{m_{\gamma'}(y_k, S_i)}{m_{\gamma'}(S_i)} + \left(n_{j,\gamma'} - \sigma_{\gamma'}\right) \frac{m_{\gamma'}(y_k, S_j)}{m_{\gamma'}(S_j)}} \quad (13)$$

   Alternatively, one can employ the steps presented in Dahl [2005] for non-conjugate cases.

   S3 Compute the Metropolis-Hastings ratio and accept η^* as the current state η with probability given by this ratio. The calculation of the Metropolis-Hastings ratio is discussed below.

3. Otherwise, i and j belong to different components in η. Propose $\eta^{\star}$ by attempting a merge move:

   M1 For convenience, let S_i and S_j denote the components in η containing i and j, respectively.

   M2 Form a merged component $S = S_i \cup S_j$.

M3 Propose the following set partition: $\eta^\star = \eta \cup \{S\} \backslash \{S_i, S_j\}$.

M4 Compute the Metropolis-Hastings ratio and accept $\eta^\star$ as the current state η with probability given by this ratio. Again, the calculation of the Metropolis-Hastings ratio is discussed below.

Computing the Metropolis Ratio The MH ratio for the SAMS sampling algorithm is given as:

$$a\left(\eta^\star|\eta\right) = \min\left[1, \frac{p\left(\eta^\star|y\right)}{p(\eta|y)} \frac{Pr\left(\eta|\eta^\star\right)}{Pr\left(\eta^\star|\eta\right)}\right]$$

where $p\left(\eta^\star|y\right)$ is the partition posterior distribution evaluated at $\eta^\star$ and $Pr\left(\eta^\star|\eta\right)$ is the probability of proposing $\eta^\star$ from the state η.

We have that $p(\eta|y) \propto p(y|\eta)p(\eta)$, where $p(\eta) = \frac{\prod_{j=1}^{K-1}(\theta_{\gamma'}+j\sigma_{\gamma'})}{(\theta_{\gamma'}+1)_{n_{\gamma'}-1}} \prod_{j=1}^{K}(1-\sigma_{\gamma'})_{n_{j,\gamma'}-1}$ is the 2PPD process EPPF and

$$p(y|\eta) = \prod_{l=1}^{K} p\left(S_l\right) = \prod_{l=1}^{K} \int \prod_{k \in S_l} F\left(y_k; \vartheta\right) P^*_{\gamma'}(\vartheta) d\vartheta = \prod_{l=1}^{K} m\left(S_l\right)$$

.

Finally, let us focus on $p(\eta^\star|\eta)$. When the proposal $\eta^\star$ is a split update, $Pr(\eta^\star|\eta)$ is merely the product of the probabilities in (13) associated with the chosen allocations. Since these two split components could only be merged in one way, $Pr(\eta|\eta^\star) = 1$. Conversely, when the proposal $\eta^\star$ is a merge update, $Pr(\eta^\star|\eta)$ is 1, but $Pr(\eta|\eta^\star)$ is the product of the probabilities in (13) associated with the allocation choices that would need to be made to obtain the split partition η, although no actually splitting is performed. Dahl underlines that it is critical that a random permutation of the indexes is used when performing this imaginary split.

Web Appendix B: Proof of Proposition 1.

We first evaluate the probability distribution of the Z_i's, partitioned into K distinct clusters with representatives located at infinitesimal intervals $\mathrm{d}x_1, ..., \mathrm{d}x_K$, around points $x_1, \ldots, x_K$, with respective multiplicities $n_1, n_2, ..., n_K$.

$$\begin{aligned}
&\mathbb{P}[Z_1^* \in \mathrm{d}x_1, \ldots, Z_K^* \in \mathrm{d}x_K, n_1, \ldots, n_K] \\
&= \mathbb{E}\left[\prod_{j=1}^{K} \left\{ w\frac{\mu_0(\mathrm{d}x_j)}{\mu_0(\mathbb{Z})} + (1-w)\frac{\mu_1(\mathrm{d}x_j)}{\mu_1(\mathbb{X})} \right\}^{n_j}\right] \\
&= \sum_{i_1=0}^{n_1} \cdots \sum_{i_K=0}^{n_K} \binom{n_1}{i_1} \cdots \binom{n_K}{i_K} w^{i_1+\cdots+i_K}(1-w)^{n-(i_1+\cdots+i_K)} \times
\end{aligned}$$

$$\mathbb{E}\left[\prod_{j=1}^{K}\left(\frac{\mu_0(\mathrm{d}x_j)}{\mu_0(\mathbb{X})}\right)^{i_j}\left(\frac{\mu_1(\mathrm{d}x_j)}{\mu_1(\mathbb{X})}\right)^{n_j-i_j}\right]$$

From Lemma 1, it follows that for any $i_j \notin \{0, n_j\}$ the expected value above vanishes. Hence, for $i_j \in \{0, n_j\}$ one has

$$\mathbb{E}\left[\prod_{j=1}^{K}\left(\frac{\mu_0(\mathrm{d}x_j)}{\mu_0(\mathbb{X})}\right)^{i_j}\left(\frac{\mu_1(\mathrm{d}x_j)}{\mu_1(\mathbb{X})}\right)^{n_j-i_j}\right] = \prod_{j=1}^{K}[P_0^*(\mathrm{d}x_j)]^{\frac{i_j}{n_j}}[P_1^*(\mathrm{d}x_j)]^{\frac{n_j-i_j}{n_j}}$$
$$\Pi_{|\boldsymbol{i}|,0}^{(\boldsymbol{n}'\boldsymbol{i})}(i_1,\ldots,i_K)\,\Pi_{K-|\boldsymbol{i}|,1}^{(n-\boldsymbol{n}'\boldsymbol{i})}(n_1-i_1,\ldots,n_K-i_K)$$

The representation in Proposition 1, then, follows when integrating out with respect to ρ and $x_1, \ldots, x_k$.

Web Appendix C: Plot of the five Scenarios considered in the simulation study

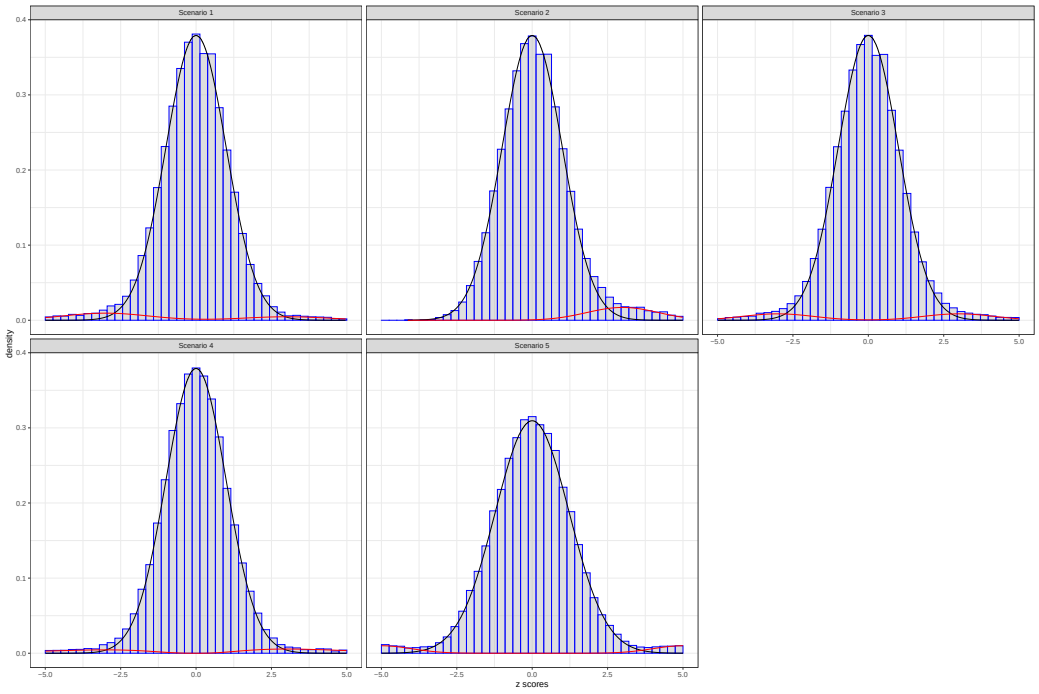

Figure 3: The five Scenarios considered in the simulation study in Section 4.1. We plot the histograms of the simulated data and superimpose the null (blue) and alternative (red) density functions.

We recall here the five scenarios that we investigate in our simulation study:

We simulate z-scores from mixture (1), where $f_0(z) = \mathcal{N}(z \mid 0, \sigma_k^2), \quad k = 1, \ldots, 5$ and for f_1 we choose:

- **Scenario 1**: $f_1(z) = 0.67 \cdot \mathcal{N}(z| -3, 2) + 0.33 \cdot \mathcal{N}(z|3, 2)$,
- **Scenario 2**: $f_1(z) = \mathcal{N}(z \mid u, 1)$ with $u \sim \text{Uniform}(2, 4)$,
- **Scenario 3**: $f_1(z) = \mathcal{N}(z \mid u,)$ with $u \sim \text{Uniform}([-4, -2] \cup [2, 4])$,
- **Scenario 4**: $f_1(z) = \text{Gamma}((-1)^v \cdot z \mid a, b)$ with $a = 4$, $b = 1$ and $v \sim \text{Bernoulli}(0.5)$,
- **Scenario 5**: $f_1(z) = 0.5 \cdot \mathcal{N}(z|5, 1) + 0.5 \cdot \mathcal{N}(z| -5, 1)$,

where $\sigma_k^2 = 1$ for $k = 1, \ldots, 4$ and $\sigma_5^2 = 1.5$. In words, f_1 is assumed asymmetric unimodal (scenario 1), symmetric bimodal (scenario 2), asymmetric bimodal (scenario 3) and symmetric bimodal with fat tails (scenario 4 and scenario 5), thus mimicking typical high-dimensional testing situations. Moreover, in scenario 5 the null distribution departs from the theoretical standard Gaussian and the alternative distribution is chosen to be easily detectable, being very separated from the null one. Figure 3 shows the histograms of data simulated under the five scenarios.

Web Appendix D: Computational Burden

We perform a simulation study where we investigate the computational time needed by the algorithm in its original specification (Pólya Urn scheme - PUS) compared to the Split-Merge (SM) alternative proposed in the previous subsection. More precisely, we keep track of the time in seconds that the model needs to run 100 iterations. For the SM case, we perform 10 SM moves per iterations, and full sweep is executed every 10 steps.

We study how the computational time varies as the sample size and the discount parameter of the null process change. These two quantities play an important role in the sampler efficiency, since the expected number of clusters grows for larger n and σ_0. In particular, $\sigma_0 > \sigma_1$ implies that the number of latent clusters generated by the null 2PPD process grows quickly, and – as a result – the algorithm becomes computationally expensive and slow. This is true, for example, not only for the sampler we initially proposed but also for slice sampling implementations. In our case, a slice sampler algorithm has a tendency to create a huge number of atoms, making the sampling unfeasible to be performed in reasonable time.

Table 3 reports the results of our comparison of PUS and SM samplers in seconds. The computational burden becomes more evident with the increase in sample size. The impact of σ_0 on the computational time is amplified with increasing sample size. We see how, for sample sizes beyond 1,000 observations, the PUS sampler becomes extremely inefficient, making inference infeasible. Relying on the SM moves considerably speeds up the algorithm. We also notice how the value of σ_0 has a small impact on the SM sampler.

		$\sigma_0 = 0.5$	$\sigma_0 = 0.75$	$\sigma_0 = 0.9$
$n = 100$	PUS	5.480	5.916	6.007
	SM	6.373	5.625	5.614
$n = 200$	PUS	12.396	14.498	15.009
	SM	10.448	10.625	10.696
$n = 500$	PUS	51.319	58.532	61.201
	SM	22.625	23.585	18.599
$n = 1,000$	PUS	186.226	221.853	236.200
	SM	54.390	52.042	42.521
$n = 2,000$	PUS	914.227	1137.689	1160.732
	SM	145.904	146.850	144.341

Table 3: Computational time in seconds for 100 iterations with the Pólya Urn Scheme (PUS) sampler, compared with the Split-Merge (SM) scheme. We investigate how the time varies as the sample size n and the discount parameter of the null process change.

Web Appendix E: Additional simulation studies

Sensitivity to discount parameters

In this Section, we study the effect of considering discount parameters σ_0, σ_1 with $\sigma_0 < \sigma_1$. More specifically, we assume $\sigma_0 = 0.1$ and $\sigma_1 = 0.75$. The remaining hyper-parameters are set according to the simulation scenarios in Section 4.1. When thresholding the BFDR at 10%, all the observations are flagged as interesting, since all the posterior probability of the alternative are too high. To exemplify, Figure 4 reports the posterior probability of the alternative for all the observations of one of the datasets in the five different scenarios. To obtain the results reported in Table 4, we set the threshold at the 1% level. We see how the model fails to recognize the two underlying distributions, since the null distribution is free to vary and even the values around zero are taken over by the alternative.

Scenario	MCC		F1		SPEC		ACC		PRE		AUC	
1	0.1569	(0.0147)	0.1409	(0.0062)	0.3823	(0.0272)	0.4114	(0.0258)	0.0760	(0.0035)	0.9189	(0.0213)
2	0.1668	(0.0136)	0.1436	(0.0066)	0.3792	(0.0312)	0.4096	(0.0296)	0.0774	(0.0038)	0.9477	(0.0168)
3	0.1664	(0.0131)	0.1468	(0.0064)	0.3724	(0.0320)	0.4042	(0.0302)	0.0793	(0.0037)	0.9448	(0.0178)
4	0.1697	(0.0168)	0.1445	(0.0094)	0.3765	(0.0459)	0.4075	(0.0436)	0.0779	(0.0055)	0.9656	(0.0100)
5	0.1157	(0.0125)	0.1183	(0.0048)	0.2138	(0.0363)	0.2531	(0.0345)	0.0629	(0.0027)	0.9867	(0.0026)

Table 4: Simulation study: sensitivity results across the five simulation scenarios considered in Section 4.1 ($\rho = 0.05$), modeled with PYs processes characterized by $\theta_0 = \theta_1 = 1$ and $\sigma_0 = 0.1 < \sigma_1 = 0.75$. The values in the table represent the average MCC and F_1 scores, the average precision (PRE), specificity (SPEC), accuracy (ACC) and the area under the curve (AUC) of the corresponding receiver operating characteristic curve, over 30 replicates with corresponding standard deviations between brackets.

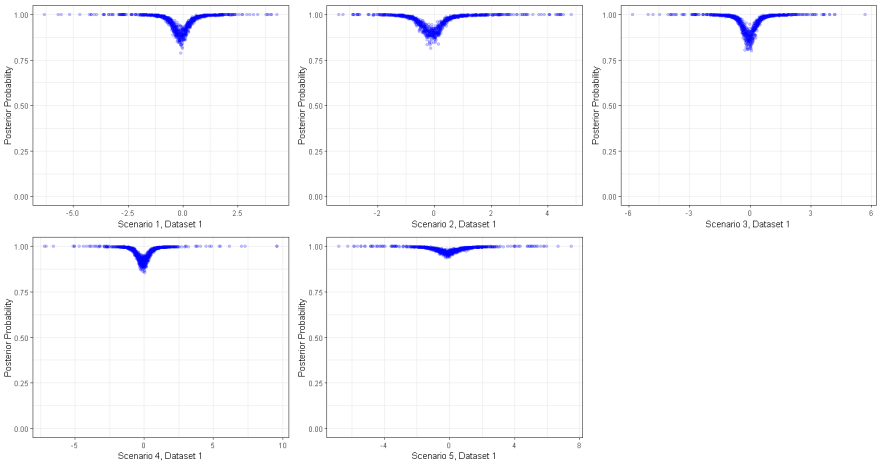

Figure 4: Posterior probability of the alternative for observations sampled in the first dataset of the five different scenarios, estimated adopting $\sigma_0 = 0.1$ and $\sigma_1 = 0.75$

Sensitivity to the sample size

We also investigate the extent by which the sample size could affect the results. More especifically, we compare the results obtained with the 2PPD model ($\sigma_0 = .75$, $\sigma_1 = 0.1$) and the different competitors on Scenario 4 and 5 for different sample sizes. We consider $n = 200, 500, 800, 1500, 2000$ for both the scenarios. Web Tables 5 and 6 present the results. We can appreciate how the results are stable throughout the different sample sizes. The symbol $-$ indicates the cases where the models failed to be estimated due to a too small sample size.

Scenario 4											
n	Index	2PPD		*locfdr*		Benjamini and Hochberg [1995]		Muralidharan [2012]		Martin and Tokdar [2012]	
200	MCC	0.7146	(0.1210)	0.6651	(0.1227)	0.7354	(0.0906)	—		0.5918	(0.1645)
	F1	0.6910	(0.1458)	0.6238	(0.1511)	0.7217	(0.1072)	—		0.5305	(0.2045)
	SPEC	0.9707	(0.0241)	0.8774	(0.0871)	0.9656	(0.0328)	—		0.9569	(0.0360)
	ACC	0.9604	(0.0703)	0.9905	(0.0522)	0.9301	(0.0976)	—		1.0000	(0.0000)
	PRE	0.9986	(0.0024)	0.9996	(0.0019)	0.9968	(0.0047)	—		1.0000	(0.0000)
	AUC	0.9767	(0.0082)	0.9733	(0.0083)	0.9775	(0.0069)	—		0.9693	(0.0096)
500	MCC	0.7042	(0.0881)	0.6609	(0.0786)	0.7547	(0.0773)	—		0.6220	(0.0917)
	F1	0.6787	(0.1054)	0.6203	(0.0999)	0.7492	(0.0842)	—		0.5702	(0.1165)
	SPEC	0.9607	(0.0240)	0.9189	(0.0481)	0.9689	(0.0182)	—		0.9491	(0.0382)
	ACC	0.9699	(0.0431)	0.9916	(0.0261)	0.9126	(0.0572)	—		0.9970	(0.0166)
	PRE	0.9991	(0.0013)	0.9997	(0.0009)	0.9966	(0.0024)	—		0.9999	(0.0004)
	AUC	0.9757	(0.0062)	0.9727	(0.0052)	0.9791	(0.0058)	—		0.9703	(0.0056)
800	MCC	0.7460	(0.0564)	0.7041	(0.0588)	0.7809	(0.0435)	0.6751	(0.1156)	0.6875	(0.0484)
	F1	0.7292	(0.0663)	0.6741	(0.0738)	0.7797	(0.0464)	0.6402	(0.1332)	0.6536	(0.0604)
	SPEC	0.9644	(0.0170)	0.9337	(0.0368)	0.9733	(0.0111)	0.9511	(0.0867)	0.9665	(0.0137)
	ACC	0.9758	(0.0263)	0.9958	(0.0129)	0.9164	(0.0549)	0.9983	(0.0089)	0.9969	(0.0118)
	PRE	0.9992	(0.0009)	0.9999	(0.0004)	0.9965	(0.0026)	0.9999	(0.0003)	0.9999	(0.0003)
	AUC	0.9786	(0.0042)	0.9756	(0.0040)	0.9809	(0.0034)	0.9740	(0.0056)	0.9744	(0.0033)
1500	MCC	0.7368	(0.0334)	0.6988	(0.0341)	0.7736	(0.0359)	0.6801	(0.0327)	0.6782	(0.0347)
	F1	0.7204	(0.0380)	0.6694	(0.0434)	0.7722	(0.0387)	0.6447	(0.0411)	0.6428	(0.0436)
	SPEC	0.9592	(0.0113)	0.9362	(0.0280)	0.9706	(0.0086)	0.9679	(0.0093)	0.9690	(0.0087)
	ACC	0.9702	(0.0228)	0.9908	(0.0172)	0.9172	(0.0370)	0.9974	(0.0100)	0.9949	(0.0139)
	PRE	0.9991	(0.0007)	0.9997	(0.0005)	0.9967	(0.0017)	0.9999	(0.0003)	0.9999	(0.0004)
	AUC	0.9778	(0.0024)	0.9751	(0.0024)	0.9804	(0.0028)	0.9738	(0.0022)	0.9737	(0.0024)
2000	MCC	0.7269	(0.0359)	0.6913	(0.0415)	0.7730	(0.0365)	0.6660	(0.0427)	0.6698	(0.0383)
	F1	0.7075	(0.0416)	0.6605	(0.0518)	0.7732	(0.0385)	0.6266	(0.0537)	0.6315	(0.0481)
	SPEC	0.9596	(0.0115)	0.9485	(0.0277)	0.9718	(0.0085)	0.9694	(0.0096)	0.9699	(0.0090)
	ACC	0.9749	(0.0197)	0.9889	(0.0167)	0.9066	(0.0392)	0.9977	(0.0068)	0.9979	(0.0065)
	PRE	0.9992	(0.0006)	0.9997	(0.0005)	0.9962	(0.0018)	0.9999	(0.0002)	0.9999	(0.0002)
	AUC	0.9771	(0.0026)	0.9746	(0.0029)	0.9803	(0.0029)	0.9729	(0.0029)	0.9731	(0.0026)

Table 5: Simulation study: sensitivity results for three different sample sizes evaluated on Scenario 4, as defined in Section 4.1 ($\rho = 0.05$). The 2PPD model is characterized by $\theta_0 = \theta_1 = 1$, $\sigma_0 = 0.1$ and $\sigma_1 = 0.75$. he values in the table represent the average MCC and F_1 scores, the average precision (PRE), specificity (SPEC), accuracy (ACC) and the area under the curve (AUC) of the corresponding receiver operating characteristic curve, over 30 replicates with corresponding standard deviations between brackets.

Scenario 5												
n	Index	2PPD		*locfdr*		Benjamini and Hochberg [1995]		Muralidharan [2012]		Martin and Tokdar [2012]	
200	MCC	0.8789	(0.0519)	0.8598	(0.0798)	0.7989	(0.0826)	—		0.8536	(0.1731)
	F1	0.8796	(0.0518)	0.8545	(0.0893)	0.7930	(0.0875)	—		0.8410	(0.2052)
	AUC	0.9981	(0.0042)	0.9855	(0.0298)	0.9981	(0.0040)	—		0.9979	(0.0042)
	PRE	0.7988	(0.0721)	0.9893	(0.0328)	0.6700	(0.1187)	—		0.9903	(0.0296)
	SPEC	0.9865	(0.0060)	0.9995	(0.0016)	0.9723	(0.0133)	—		0.9995	(0.0016)
	ACC	0.9863	(0.0063)	0.9877	(0.0065)	0.9730	(0.0132)	—		0.9882	(0.0116)
500	MCC	0.8606	(0.0406)	0.8668	(0.0600)	0.7891	(0.0462)	—		0.8982	(0.0463)
	F1	0.8624	(0.0404)	0.8638	(0.0652)	0.7827	(0.0496)	—		0.8987	(0.0480)
	AUC	0.9976	(0.0016)	0.9973	(0.0050)	0.9987	(0.0013)	—		0.9986	(0.0015)
	PRE	0.7797	(0.0594)	0.9865	(0.0357)	0.6479	(0.0658)	—		0.9794	(0.0357)
	SPEC	0.9853	(0.0049)	0.9993	(0.0019)	0.9696	(0.0082)	—		0.9989	(0.0019)
	ACC	0.9844	(0.0050)	0.9877	(0.0052)	0.9709	(0.0081)	—		0.9904	(0.0042)
800	MCC	0.8834	(0.0312)	0.8572	(0.0547)	0.7859	(0.0414)	0.8530	(0.0509)	0.8896	(0.0421)
	F1	0.8854	(0.0302)	0.8538	(0.0595)	0.7795	(0.0456)	0.8497	(0.0551)	0.8896	(0.0439)
	AUC	0.9984	(0.0018)	0.9954	(0.0075)	0.9985	(0.0018)	0.9983	(0.0020)	0.9984	(0.0017)
	PRE	0.8093	(0.0387)	0.9850	(0.0226)	0.6459	(0.0624)	0.9866	(0.0202)	0.9824	(0.0199)
	SPEC	0.9878	(0.0029)	0.9993	(0.0010)	0.9707	(0.0079)	0.9995	(0.0008)	0.9992	(0.0009)
	ACC	0.9873	(0.0035)	0.9873	(0.0046)	0.9716	(0.0075)	0.9870	(0.0042)	0.9900	(0.0036)
1500	MCC	0.8869	(0.0179)	0.8763	(0.0452)	0.7799	(0.0288)	0.8619	(0.0409)	0.8954	(0.0333)
	F1	0.8897	(0.0177)	0.8753	(0.0485)	0.7727	(0.0316)	0.8599	(0.0437)	0.8966	(0.0338)
	AUC	0.9984	(0.0013)	0.9964	(0.0047)	0.9986	(0.0009)	0.9986	(0.0009)	0.9986	(0.0009)
	PRE	0.8218	(0.0275)	0.9836	(0.0165)	0.6337	(0.0424)	0.9865	(0.0162)	0.9763	(0.0236)
	SPEC	0.9887	(0.0022)	0.9993	(0.0007)	0.9691	(0.0054)	0.9994	(0.0007)	0.9989	(0.0011)
	ACC	0.9878	(0.0021)	0.9888	(0.0039)	0.9702	(0.0052)	0.9875	(0.0035)	0.9904	(0.0030)
2000	MCC	0.8920	(0.0198)	0.8715	(0.0413)	0.7853	(0.0237)	0.8579	(0.0365)	0.8893	(0.0282)
	F1	0.8952	(0.0191)	0.8701	(0.0451)	0.7789	(0.0260)	0.8552	(0.0396)	0.8901	(0.0290)
	AUC	0.9982	(0.0013)	0.9958	(0.0049)	0.9984	(0.0012)	0.9983	(0.0013)	0.9982	(0.0014)
	PRE	0.8350	(0.0255)	0.9847	(0.0154)	0.6426	(0.0362)	0.9892	(0.0111)	0.9806	(0.0176)
	SPEC	0.9899	(0.0018)	0.9993	(0.0007)	0.9708	(0.0044)	0.9996	(0.0005)	0.9991	(0.0008)
	ACC	0.9887	(0.0021)	0.9885	(0.0034)	0.9718	(0.0041)	0.9874	(0.0030)	0.9900	(0.0024)

Table 6: Simulation study: sensitivity results for five different sample sizes evaluated on Scenario 5, as defined in Section 4.1 ($\rho = 0.05$). The 2PPD model is characterized by $\theta_0 = \theta_1 = 1$, $\sigma_0 = 0.1$ and $\sigma_1 = 0.75$. he values in the table represent the average MCC and F_1 scores, the average precision (PRE), specificity (SPEC), accuracy (ACC) and the area under the curve (AUC) of the corresponding receiver operating characteristic curve, over 30 replicates with corresponding standard deviations between brackets.

Web Appendix F: Microbiome data: list of differentially abundant taxa

Table 7: Microbiome data case study: differentially abundant taxa with negative z-scores indicating less abundance in the children with moderate to severe diarrhea. Most are well known commensal bacteria, e.g. *Prevotella* spp. and *Clostridium* spp. Posterior probability that the z-score belongs to the non-null group is given for each taxa. The dotted line highlights the difference between the genes flagged as relevant by our method and the ones found with the *locfdr* model.

Taxon	z-score	$p(K_i = 1\|\text{data})$	Efron LocFdr
Prevotella copri	-10.13	1.00	0.99
Prevotella sp. DJF_RP53	-9.76	1.00	0.98
Prevotella sp. BI-42	-9.72	1.00	0.98
Prevotella sp. DJF_B112	-9.64	1.00	0.98
Clostridium lituseburense	-8.53	1.00	0.86
Clostridium paraputrificum	-7.78	1.00	0.62
Faecalibacterium prausnitzii	-7.49	1.00	0.50
Prevotella sp. oral clone BP1-28	-7.38	1.00	0.46
Clostridium bartlettii	-7.01	1.00	0.33
Clostridium sp. FRC_C11	-6.80	1.00	0.27
Faecalibacterium sp. DJF_VR20	-6.59	1.00	0.23
Clostridium disporicum	-6.33	1.00	0.19
Collinsella sp. CB20	-6.26	1.00	0.19
Ruminococcus gnavus	-6.02	1.00	0.18
Bacteroides fragilis	-5.90	1.00	0.18
Clostridium butyricum	-5.90	1.00	0.18
Enterococcus sp. L2	-5.78	1.00	0.18
Prevotella intermedia	-5.68	1.00	0.18
Clostridium glycolicum	-5.29	0.99	0.20
Bacteroides sp. CJ78	-5.22	0.99	0.21
Collinsella aerofaciens	-5.19	0.99	0.21
Eubacterium rectale	-5.06	0.99	0.21
Bacteroides xylanisolvens	-4.95	0.98	0.21
Clostridium hathewayi	-4.86	0.98	0.22
Collinsella sp. HA6	-4.69	0.97	0.21
Turicibacter sanguinis	-4.68	0.97	0.21
Clostridium sp. CJ66	-4.66	0.97	0.21
Prevotella sp. oral clone AO009	-4.65	0.97	0.21
Enterococcus gallinarum	-4.59	0.96	0.21
Megasphaera sp. TrE9262	-4.53	0.96	0.20
Bacteroides ovatus	-4.52	0.96	0.20
Clostridium difficile	-4.30	0.95	0.19

Table 8: Microbiome data case study: differentially abundant taxa with positive z-scores indicating greater abundance in the children with moderate to severe diarrhea. Most are well known pathogenic bacteria, e.g. *Shigella* spp. and *E. coli*. Posterior probability that the z-score belongs to the non-null group is given for each taxa. The dotted line highlights the difference between the genes flagged as relevant by our method and the ones found with the *locfdr* model.

Taxon	z-score	$p(K_i = 1\|\text{data})$	Efron LocFdr
Escherichia coli	8.48	1.00	0.83
Streptococcus sp. C101	7.66	1.00	0.70
Haemophilus haemolyticus	7.62	1.00	0.69
Streptococcus mitis	7.48	1.00	0.65
Erwinia chrysanthemi	7.18	1.00	0.58
Streptococcus sp. oral clone ASCE09	7.10	1.00	0.55
Enterobacter cloacae	6.87	1.00	0.49
Acinetobacter sp. SF6	6.56	1.00	0.40
Granulicatella sp. oral clone ASCG05	6.34	1.00	0.33
Streptococcus sp. oral clone ASCC04	6.18	1.00	0.28
Shigella boydii	5.93	1.00	0.20
Streptococcus sp. oral clone ASCC01	5.82	1.00	0.17
Streptococcus peroris	5.81	1.00	0.17
Rothia mucilaginosa	5.76	1.00	0.15
Streptococcus oralis	5.75	1.00	0.15
Escherichia sp. oral clone 3RH-30	5.58	1.00	0.11
Citrobacter freundii	5.58	1.00	0.11
Granulicatella adiacens	5.54	1.00	0.10
Streptococcus sanguinis	5.47	1.00	0.08
Escherichia albertii	5.24	1.00	0.03
Escherichia sp. EMB 210	5.08	1.00	0.01
Granulicatella elegans	5.04	1.00	0.00
Streptococcus pneumoniae	5.03	0.99	0.00
Fusobacterium nucleatum	5.03	1.00	0.00
Serratia marcescens	4.97	1.00	0.00
Streptococcus sp. oral strain T4-E3	4.86	0.99	0.00
Streptococcus sp. oral clone DP009	4.84	0.99	0.00
Shigella sonnei	4.79	0.99	0.00
Fusobacterium periodonticum	4.76	0.99	0.00
Neisseria sp. oral clone BP2-82	4.62	0.99	0.00
Actinobacillus pleuropneumoniae	4.59	0.99	0.00
Streptococcus parasanguinis	4.52	0.99	0.00
Streptococcus sp. C163	4.50	0.99	0.00
Fusobacterium sp. oral clone BS011	4.48	0.99	0.00
Haemophilus sp. oral clone BJ021	4.39	0.98	0.00
Streptococcus sp. oral clone BP1-49	4.25	0.98	0.00
Abiotrophia defectiva	4.24	0.98	0.00
Streptococcus sp. oral clone MCE7_144	4.19	0.98	0.00
Haemophilus influenzae	4.11	0.97	0.00
Campylobacter jejuni	4.11	0.97	0.00
Citrobacter sp. SVUB3	4.07	0.97	0.00
Enterobacter sp. CRRI 3	3.89	0.95	0.00

Web Appendix G: Interesting Biological Findings

Among the species which were identified by our method as having significantly less abundance in MSD children, we found *Prevotella* species and *Clostridium* species (see Table 1 in Web Appendix C). *Prevotella* spp. are common bacteria in the gut and are commonly found in children from rural and underdeveloped areas [Di Paola et al., 2010] as well as children whose diets predominantly consist of carbohydrates and fiber [Chen et al., 2011]. Thus the severely decreased abundance of the *Prevotella* spp. is reasonable in light of the gastrointestinal disruption the children experienced. As for the *Clostridium* spp., it is well-known that *C. difficile* is a toxigenic bacteria in adults but it is also found asymptomatically in large proportions in infants and neonates [Jangi and Lamont, 2010]. Another interesting species is *Megasphaera*, which was recently suggested for reclassification to *Clostridium* [Yutin and Galperin, 2013]. Finally, *Eubacterium rectale*, *Bacteroides*, and *Faecalibacterium prausnitzii*, have all been shown a marked reduction in concentrations in patients affected by chronic idiopathic diarrhea [Swidsinski et al., 2008].

Of the species identified as significantly more abundant in the MSD children, many of them belong to the *Streptococcus* species. Some *Streptococcus* species are well known human pathogens causing conjunctivitis, respiratory infections and urinary tract infections. Other species in the genus are opportunistic pathogens, meaning they are asymptomatically present in healthy individuals but will flourish in individuals with weakened immune systems such as the patients in this dataset. The pathogenic genus *Shigella* is present and is well-known for causing dysentery. It has been suggested that the *Shigella* spp. are closely related to another well-known pathogen, *Escherichia coli* [Lan and Reeves, 2002] which is also differentially abundant in these patients. A *Granulicatella* species has also been identified as differentially abundant. However, these bacteria are usually implicated in childhood infective endocarditis or infection of the heart.